Algal Research 35 (2018) 33–49

Contents lists available at ScienceDirect

Algal Research

journal homepage: www.elsevier.com/locate/algal

# Orchestration of transcriptome, proteome and metabolome in the diatom *Phaeodactylum tricornutum* during nitrogen limitation

Ilse M. Remmers[a], Sarah D'Adamo[a,*], Dirk E. Martens[a], Ric C.H. de Vos[b], Roland Mumm[b], Antoine H.P. America[b], Jan H.G. Cordewener[b], Linda V. Bakker[b], Sander A. Peters[b], René H. Wijffels[a,c], Packo P. Lamers[a]

[a] Bioprocess Engineering & AlgaePARC, Wageningen University and Research, P.O. Box 16, 6700 AA Wageningen, the Netherlands
[b] BU Bioscience, Wageningen University and Research, P.O. Box 16, 6700 AA Wageningen, the Netherlands
[c] Biosciences and Aquaculture, Nord University, N-8049 Bodø, Norway

ARTICLE INFO

*Keywords:*
Triacylglycerol
Lipids
Diurnal metabolism
Omics
Diatoms
Mitochondrion

ABSTRACT

Nitrogen deprivation increases the triacylglycerol (TAG) content in microalgae but also severely decreases the growth rate. Most approaches that attempted to increase TAG productivity by overexpression or knockdown of specific genes related to the regulation of the lipid synthesis have reported only little success. More insight into the molecular mechanisms related to lipid accumulation and impaired growth rate is needed to find targets for improving TAG productivity. By using the emerging "omics" approach, we comprehensively profiled the physiology, transcriptome, proteome and metabolome of the diatom *Phaeodactylum tricornutum* during steady state growth at both nitrogen limited and replete levels during light:dark cycles. Under nitrogen limited conditions, 22% (2699) of the total identified transcripts, 17% (543) of the proteins and 44% (345) of the metabolites were significantly differentially regulated compared to nitrogen replete growth conditions. Although nitrogen limitation was responsible for the majority of significant differential transcript, protein and metabolite accumulation, we also observed differential expression over a diurnal cycle. Nitrogen limitation mainly induced an upregulation of nitrogen fixation, central carbon metabolism and TCA cycle, while photosynthetic and ribosomal protein synthesis are mainly downregulated. Regulation of the lipid metabolism and the expression of predicted proteins involved in lipid processes suggest that lipid rearrangements may substantially contribute to TAG distribution. However, TAG synthesis is also limited by the reduced carbon flux through central metabolism. Future strain improvements should therefore focus on understanding and improving the carbon flux through central carbon metabolism, selectivity and activity of DGAT isoforms and lipase enzymes.

## 1. Introduction

Microalgae are regarded as a promising production platform for specialty fatty acids and the bulk production of triacylglycerol (TAG) for the biofuel industry [1–5]. Currently, microalgae are already commercially applied for the heterotrophic production of fatty acids for the food- and feed industry [6,7]. However, microalgae are also able to grow phototrophically, directly converting sunlight into chemical energy by the fixation of $CO_2$ into biomass and useful products like TAG. TAG accumulation occurs when microalgae are exposed to suboptimal growth conditions (e.g., nitrogen deprivation). Microalgae can accumulate lipids up to 60% of dry weight at the expense of growth [8,9]. The decreased photosynthetic efficiency under suboptimal growth condition is one of the key limitations in commercializing photosynthetic algal bulk lipid production [10].

A lot of research has been published on the effect of nitrogen (N) deprivation on lipid accumulation in different microalgal strains [8,11,12]. However, the exact mechanism for the induction of TAG synthesis and the loss of photosynthetic efficiency under N deprivation is not elucidated yet. Moreover the influence of light:dark (LD) cycles, which are present at (large scale) outdoor production, are not known. The increasing availability of sequenced genomes and molecular techniques allowed more studies to focus on the molecular mechanisms behind the regulation of TAG accumulation in microalgae. Rational (metabolic) engineering strategies to improve TAG production, however, are still ambiguous due to lacking understanding of microalgal lipid metabolism [13–16]. With the rapid development of 'omics' technologies (e.g., transcriptomics, proteomics, metabolomics), new

* Corresponding author.
*E-mail address:* sarah.dadamo@wur.nl (S. D'Adamo).

https://doi.org/10.1016/j.algal.2018.08.012
Received 12 February 2018; Received in revised form 31 July 2018; Accepted 9 August 2018

possibilities arise, allowing a more comprehensive description of microalgal metabolism and its regulation.

While the effect of N deficiency on microalgal metabolism has been predominantly studied at the transcriptomic level, the effects on protein and metabolite levels are often neglected [17–22]. Some regulated changes on the transcriptome expression level may not lead to comparable changes in the protein or metabolite level [23,24]. An 'integrated' omics approach may provide a complete picture and novel insights on the orchestration of the stress response in a cell. To our knowledge, only few microalgal studies exploited the combination of transcriptome, proteome and/or metabolome data [25–27]. For example, Schmollinger et al. (2014) identified a target to increase the nitrogen-use efficiency in the nitrogen-starved *Chlamydomonas reinhardtii* [27].

Most of the microalgal 'omics' studies, focussing on improving lipid productivity, have focussed on N starved batch cultures [20,25,26,28]. Such processes allow studying molecular mechanism over time and thus giving insight in the order of regulatory events related to lipid induction. However, the main disadvantage of a batch system is the continuous change in the culturing conditions (e.g., light per cell, progressive cell death under N starvation) that can influence the measurements and the gene expression levels, which may not be directly correlated with N starvation treatment. Synchronized continuous cultures can be used to study single parameter variations, such as the impact of LD cycles, N deficiency or iron deficiency [28–30].

The aim of this study is to obtain a comprehensive insight into the metabolism of TAG production induced by N limitation at the transcriptome, proteome and metabolome level under LD cycles. N limitation was induced in continuous, turbidostat controlled, photobioreactors that allow highly reproducible culture conditions with simultaneous growth and TAG production in the marine diatom *Phaeodactylum tricornutum*. Cultures were acclimated to a 16:8 h LD cycle and samples were taken during both the light and right after the dark period for the analysis of biomass, transcriptome, proteome and metabolome. *P. tricornutum* is considered as a model fusiform diatom for the study of physiology, evolution and biochemistry [31]. *P. tricornutum* is also able to accumulate significant amount of lipids (up to 23% w/w during nutrient stress conditions) and it has therefore been proposed as a commercially exploitable source of oil and polyunsaturated fatty acids (such as ω-3 eicosapentaenoic acid, EPA) for nutraceuticals and feed applications [32]. Moreover, the availability of the whole genome sequence and molecular toolboxes and the stable transgene expression reported are making this diatom an attractive system for genetic engineering [15,33–41]. This microalgal strain therefore serves as a solid and interesting system to better understand the cellular responses related to N deprivation and the trade-off between growth and lipid accumulation.

## 2. Material and methods

### 2.1. Strain, medium and precultivation

*Phaeodactylum tricornutum* SAG1090-1b was obtained from the Culture Collection of Algae Göttingen University (Sammlung von Algenkulturen, Göttingen, Germany). Liquid cultures were maintained in a controlled incubator (25 °C, 30–40 μmol $m^{-2} s^{-1}$, 16:8 h light:dark (LD) cycle, 100 rpm, enriched air with 2% $CO_2$) in 250 ml Erlenmeyer flasks containing 100 ml of filter sterilized (pore size 0.2 μm) defined medium. The medium was designed to reach a biomass concentration of 2.5 g $L^{-1}$ and consisted of 252 mM NaCl, 16.8 mM $KNO_3$, 3.5 mM $Na_2SO_4$, 100 mM, 2-[4-(2-hydroxyethyl)piperazin-1-yl]ethanesulfonic acid (HEPES), 5 mM $MgSO_4$ $7H_2O$, 2.4 mM $CaCl_2$ $2H_2O$, 2.5 mM $K_2HPO_4$, 10 mM $NaHCO_3$, 28 μM NaFeEDTA, 80 μM $Na_2EDTA$ $2H_2O$, 19 μM $MnCl_2$ $4H_2O$, 4 μM $ZnSO_4$ $7H_2O$, 1.2 μM $CoCl_2$ $6H_2O$, 1.3 μM $CuSO_4$ $5H_2O$, 0.1 μM $Na_2MoO_4$ $2H_2O$, 0.1 μM Biotin, 3.7 μM vitamin B1 and 0.1 μM vitamin B12. The pH was adjusted with KOH to pH 7.2. Prior to the start of the experiments, cultures were transferred to an incubator with a light intensity of 180 μmol $m^{-2} s^{-1}$, a 16:8 h LD cycle and a headspace enriched with 2.5% $CO_2$ to reach the desired inoculation cell density.

### 2.2. Photobioreactor setup and experimental conditions

*P. tricornutum* was cultivated aseptically in a flatpanel airlift-loop reactor with a working volume of 1.7 L and a light path of 0.02 m (Labfors 5 Lux, Infors HT, Switserland). A similar reactor setup was described previously by Remmers et al. [42]. Cultures were continuously purged with 1.7 L $min^{-1}$ air enriched with 1% $CO_2$. The temperature was controlled at 20 °C and the pH was maintained at 7.2 using 5% $H_2SO_4$. 1–2 drops of 1%*w*/w antifoam (Antifoam B, Baker, the Netherlands) were added once per day. Light was provided by 260 LED lamps with a warm white spectrum (450–620 nm) at the culture side of the reactor. As the culture was exposed to 16:8 h light dark (LD) cycles, a black cover was placed on the rear of the reactor to prevent external light falling on the culture. After inoculation, the light intensity falling through the back side of the culture was continuously measured by a light meter (LI-250, Licor, USA). The reactor was inoculated at 0.5 g dry weight $L^{-1}$ at an incident light intensity of 50 μmol $m^2 s^{-1}$ and along with cellular growth the incident light intensity was stepwise increased until it reached the final set point of 260 μmol $m^2 s^{-1}$. Hereafter, continuous turbidostat control was initiated. The culture was diluted with fresh medium (containing no nitrogen) when the outgoing light intensity dropped below 10 μmol $m^2 s^{-1}$. Control was only active during the light period. Because the light meter has stable sensitivity for all wavelengths in the visible light range, overall light absorption by the culture remained at the fixed setting regardless of any change in spectral absorption due to alteration of pigmentation and/or size of antenna. The culture was exposed to two feeding regimes using a separate nitrogen (N) feed (Fig. 1A): N replete growth (control experiment, nitrogen supply rate of 0.11 gN $day^{-1}$) and N limited growth (0.02 gN $day^{-1}$). Under N replete conditions more nitrogen was added than consumed by the algae, resulting in an excess of nitrogen in the culture supernatant. The medium composition was kept equal to that of the preculture except for HEPES (0 mM) and $KNO_3$. The dilution medium contained no $KNO_3$ while the separate nitrogen feed medium contained either 37.5 mM (control experiment) or 21.3 mM (N limitation) $KNO_3$.

### 2.3. Reproducibility and sampling

Reproducibility of each experimental condition (e.g., control and N limited experiment) was verified by running 4 independent replicates. Each experiment was sampled daily at a fixed time point to monitor growth. Steady state was defined as a constant dilution rate and stable biomass concentration, averaged over 24 h periods, for at least 6 consecutive days. During steady state, 24 h overflow was collected on ice and used to determine the dilution rate and average growth rate per day.

Samples of the overflow were taken to determine biomass concentration ($C_{x,OF}$), absorption coefficient, and the macromolecular biomass composition (TAG, carbohydrates, protein, ash), as described by Remmers et al. [42]. Productivity ($r_i$) and yield ($Y_{i,ph}$) on light of biomass and TAG were calculated from the 24 h averaged dilution rate ($D_{24}$), concentration of biomass or TAG in the 24 h collected overflow ($C_{i,OF}$) and the photon supply rate ($r_{ph}$):

$$r_i = D_{24} \cdot C_{i,OF} \quad (1)$$

$$Y_{i,ph} = \frac{r_i}{r_{ph}} \quad (2)$$

The photosynthetic conversion efficiency (in % of the absorbed photons) was calculated using Eq. 3. Biomass was divided in functional

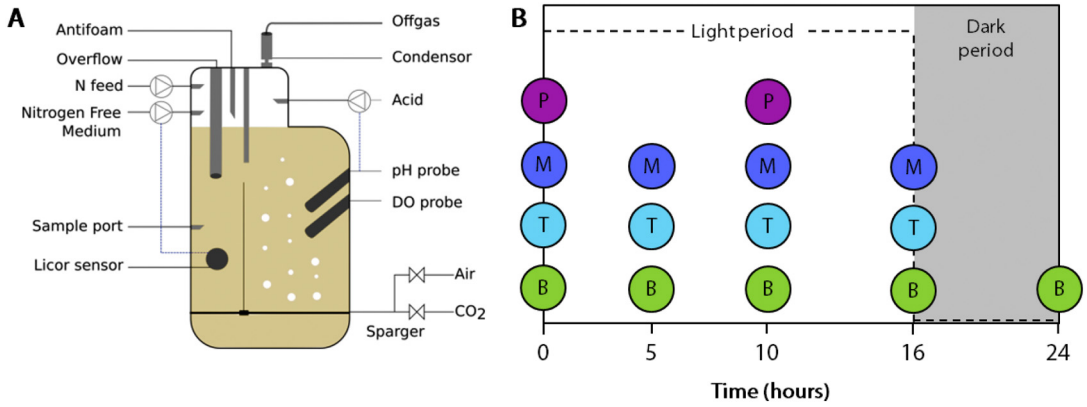


**Fig. 1.** Experimental setup (A) and sampling scheme (B). 8 independent cultures were exposed to either nitrogen limited ($N = 4$) or nitrogen replete (control; $N = 4$) continuous growth conditions. When the culture reached steady state, samples were taken at 5–6 h intervals for biomass composition (B), proteome (P), metabolome (M) and transcriptome (T) analysis. Light was always supplied in a 16 h:8 h LD cycle with the lamps either switched on at a fixed intensity of 260 μmol $m^2 s^{-1}$ or switched off (dark period; shaded areas).

biomass, TAG and storage carbohydrates. The theoretical yields of TAG (1.33 g TAG $mol^{-1}$ photon), storage carbohydrates (3.24 g storage carbohydrates $mol^{-1}$ photon) and functional biomass (1.63 g biomass $mol^{-1}$ photon) on photons were derived using a simplified metabolic flux model [43–45].

$$\text{photosynthetic conversion efficiency}\,(\%) = \frac{\frac{r_{TAG}}{1.33} + \frac{r_{carbohydrates}}{3.24} + \frac{r_{fuctional\ biomass}}{1.63}}{r_{ph}} \cdot 100 \quad (3)$$

To study diurnal fluctuations, each culture was also sampled directly from the culture broth during a 24 h cycle with 5–6 h intervals (Fig. 1B). These samples were analysed for biomass composition (e.g., TAG, membrane lipids, protein, total carbohydrates, ash) [42] and for transcriptome, proteome and metabolome analysis. Biomass for transcriptome, proteome and metabolome analysis was immediately centrifuged (4200 rpm, 1 min, 0 °C, supernatant discarded), flash frozen in liquid nitrogen and kept at −80 °C until analysis. Pellets for metabolomics analysis were freeze-dried prior to metabolite extraction.

### 2.4. Transcriptomics

#### 2.4.1. RNA isolation and sequencing

Pelleted algae cultures were homogenised in liquid nitrogen by grinding. The ruptured cells were incubated in 400 μl TriPure (Roche) for 30 min on a rotor at RT. Subsequently, total RNA was isolated using Direct-Zol RNA Miniprep kit (Zymo Research) according to the manufacturer's instructions. Finally the RNA was eluted from the column in 2 steps with 50 μl DNAse/RNase-free water. To check the RNA quality, approximately 10 μl was loaded on 1.5% agarose gel. Yield and purity were subsequently analysed by determining OD260/230 ratio using Nanodrop (Thermo Scientific). The polyA-RNA was recovered using an oligo-dT beads capture (Tru-Seq, Illumina). The RNA was converted into cDNA from which paired end sequence libraries were constructed that were subsequently sequenced with Illumina HiSeq 2500 sequence technology according to protocols provided by Illumina.

#### 2.4.2. RNA transcriptome, differential expression and gene annotation

The re-annotated reference genome for *P. tricornutum* JGI genebuild (Ensembl build 29, 2015) was retrieved from EnsemblProtist (http://protists.ensembl.org/Phaeodactylum_tricornutum/Info/Index). To determine RNA expression levels of nitrogen replete (N+) and nitrogen limited samples (N-), RNA-seq data were mapped against the annotated reference genome with CLC Genomics Server 7.5.1 software (http://CLCbio.com) using the following parameter settings; Mapping type = Map to gene regions only (fast mode), Mismatch cost = 2, Insertion cost = 3, Deletion cost = 3, Length fraction = 0.9, Similarity fraction = 0.8, Global alignment = No, Auto-detect paired distances = Yes, Strand specific = Both, Maximum number of hits for a read = 10, Count paired reads as two = No, Expression value = RPKM, Calculate RPKM for genes without transcripts = No, Create report = Yes, and Create fusion gene table = No, Create list of unmapped reads = Yes.

Subsequently, a multigroup experiment for sample sets was designed and compared for N replete (N+; control) versus N limitation (N−) at $t = 0$, and N+ versus N− at $t = 10$ using CLC Genomics Workbench 9.5.3 software. Original expression data was normalised using Quantile normalization. Subsequently, the normalized expression values were corrected for multiple testing using false discovery rate (FDR) correction. The following additional parameter settings were used for differential gene expression analysis in CLC; Total count filter cutoff = 5.0, Estimate tagwise dispersions = Yes.

Gene ontology annotation were retrieved with the ensembl REST api http://rest.ensemblgenomes.org. Additional annotation was based on protein sequences by extracting coding sequences from the annotated reference genome from *P. tricornutum* in CLC. Briefly, 11,522 CDS sequences with an ATG start codon from a total of 12,178 extracted elements were translated into proteins using a standard translation table. Next, predictive information on proteins was retrieved using InterProScan 5.16–55.0 screening against ProDom, HAMAP, Panther, SMART, SuperFamily, PRINTS, PIRSF, Pfam, Gene3d, Coils, TIGRFAM, and PrositePatterns databases. Subsequently, KEGG identifiers and additional gene ontology annotations were retrieved from Interproscan XML output.

### 2.5. Proteomics

#### 2.5.1. Protein extraction and analysis

Pelleted diatom cultures were lysed by addition of 1 ml of chloroform:methanol (1:2 v/v) and homogenised by vigorous shaking in FastPrep (2 × 20 s, position 5). After centrifugation (16,000 *g*, 10 min at RT) the supernatant was removed. This homogenisation and extraction was repeated 2 more times. Pellet material was dried in a vacuum centrifuge (SpeedVac) and was subsequently resuspended in 0.5 ml of 8 M urea, 5 mM DTT in 0.1 M ammonium bicarbonate pH 7 (ABC) with vigorous shaking in FastPrep (2 times 20 s, position 5) and 9 h rotating incubation at 37 °C. Iodoacetamide was added (15 μl of a 0.5 M stock) for alkylation of free sulfhydryl groups (cysteine and quenching of DTT, overnight incubation). After centrifugation (16,000 *g*, 10 min at RT) the supernatant was transferred to a fresh Eppendorf tube. The pellet was re-extracted twice with 0.5 ml 0.1 M ABC. The supernatants were pooled with the first (urea) extract. Protein

content was determined by Qubit Fluorometer protein assay (ThermoFisher scientific, product Q33211). An aliquot equivalent to 50 µg of protein was taken and diluted again with equal volume of 0.1 M ABC before 0.5 µg trypsin (Promega Proteomics grade) was added. Digestion was incubated overnight at 37 °C and stopped by adding 3 µl 10% trifluoro-acetic acid. Peptides were purified by solid-phase extraction (SPE) in Waters OASIS HLB micro-elution plates. Eluted peptides were dried by SpeedVac centrifugation and dissolved in 2% acetonitrile, 20 mM ammonium formate pH 10. Approximately 1 µg aliquot was injected on a 2D-nanoAcquity LC system with 2 step peptide capture and elution in four subsequent fractions. In short, peptides were first loaded onto an XBridge Peptide BEH C18 NanoEase column and subsequently eluted with steps of 15%, 19%, 25% and 65% acetonitrile in 20 mM ammonium formate pH 10, on-line diluted 10 fold with 2% acetonitrile in 0.1% formic acid (pH 2), and peptides were trapped on a second trap column nanoACQUITY HSS T3 (1.8 µm particles; 2 cm × 100 µm). Subsequently, per fraction an elution gradient was performed over analytical nanoACQUITY HSS T3 column (1.8 µm particles; 15 cm × 75 µm) using a 120 min gradient with separation between 5% to 40% acetonitrile in 100 min followed by a steep gradient to 80% for washing and return to 2% acetonitrile, all at a flow rate of 300 µl/min. Eluting peptides were on-line injected to a Q-Exactive Plus FTMS instrument (ThermoFisher Scientific). The Q-Exactive was operated in Data Dependent Analysis (DDA) positive ESI mode for automated MS/MS acquisition. Settings were: MS1: resolution = 70 k, AGC target = 3e6, MaxIT = 50mS and scan range 400–1500 *m/z*.; MS2: resolution = 35 k, AGC target = 1e5, MaxIT = 110mS, loop count = 8, ion isolation width 1.6 *m/z* no offset, NCE = 28, centroid mode and automatic scan range from 140 *m/z* upwards. Charge exclusion was set to include only 2, 3 and 4+ charged ions, preferred peptide match, excluded isotopes and dynamic exclusion during 30 s.

LC-MS/MS raw data files were processed using MaxQuant (version 1.5.3.) using carbamidomethylation of cysteine as fixed and oxidized methionine as variable modifications. Searches were performed with the proteome equivalent of *P. tricornutum* JGI genebuild (Phatr3 Ensembl build 29, 2015) retrieved from EnsemblProtist (http://protists.ensembl.org/Phaeodactylum_tricornutum/Info/Index). During processing, the data were re-calibrated, aligned, matched between runs and normalised using the LFQ quantitation algorithm [46,47]. The resulting ProteinTable (Supplemental digital material: Appendix B) was loaded, filtered and visualised using Perseus software [48].

## 2.6. Metabolomics

### 2.6.1. Metabolite extraction

Lipid-soluble, apolar compounds were extracted by mixing 25 mg freeze-dried algae with 4.6 ml of methanol/chloroform (1:1 v/v) containing 0.1% (w/v) butylhydroxytoluene as antioxidant and 10 µM of 1,2-didecanoyl-sn-glycero-3-phosphocholine as internal standard in a 10 ml glass tube. The mixture was sonicated for 15 min, crushed with a glass rod and again sonicated for 15 min. After centrifugation, 400 µl of the supernatant was transferred to an Eppendorf tube, dried in a speed-vac and dissolved in 1 ml of ethanol, after which the sample was sonicated for 5 min and centrifuged once more before transferring to an HPLC glass vial for LCMS analysis of the extracted apolar compounds.

Polar compounds were extracted using a protocol similarly as described by Carreno-Quintero et al. [49]. In brief, 15 mg of freeze-dried algae were mixed 210 µl of 80% methanol, containing ribitol (32 ng µl$^{-1}$) as an internal standard, in an Eppendorf tube. Samples were vortexed, sonicated for 15 min and centrifuged, after which 125 µl was transferred into a new Eppendorf tube containing 188 µl ice-cold $H_2O$ and 94 µl ice-cold chloroform. After vortexing, sonication and centrifugation, 50 µl of the upper polar phase was taken and dried in a speed-vac before derivatization and injection into the by GCMS.

### 2.6.2. Untargeted metabolite profiling

Apolar compounds present in the crude methanol/chloroform extracts were detected by high resolution LCMS using an Acquity UPLC (Waters) connected to an LTQ-Orbitrap XL hybrid mass spectrometer (Thermo). A Waters Acquity HSS T3 column (1.8 µm particles; 2.1 × 150 mm) at 55 °C was used to separate compounds. A solvent gradient of 20% acetonitrile in water containing 10 mM ammoniumacetate and 0.1% formic acid (eluent A) and 10% acetonitrile in isopropanol containing 10 mM ammoniumacetate and 0.1% formic acid (eluent B) was used, starting with an increase from 35 to 70% B in 3 min, then from 70 to 85% B in 6 min and from 85 to 90% B in 13 min, followed by a washing step at 90% B for another 5 min; the flow rate was 200 µl/min. Masses were recorded at a resolution of 60,000 FWHM in positive electrospray ionization mode and in the *m/z* range of 112–1400. Mass calibration and other settings of the LTQ-Orbitrap were as described by [50].

Polar compounds were analysed by GCMS after automated TMS-derivatization of the dried polar extract, as described by Carreno-Quintero et al. [49]. A series of alkanes (C10–C32) was automatically added to each sample to calculate retention indices of all eluting compounds using a third order polynomial function.

### 2.6.3. Metabolomics data processing

Raw mass spectrometry data from both LCMS and GCMS analyses were processed in an essentially untargeted manner using an in-house developed dedicated workflow, which consists of applying MetAlign software [51] for noise estimation, peak picking and alignment, selecting for reproducible signals, i.e. being present in at least 3 samples with an intensity of at least 15 times the local noise, and MSClust software [52] to cluster all mass signals originating from the same metabolite, including fragments, adducts and isotopes. The resulting metabolite tables, containing the relative signal intensity of each compound detected in each sample analysed, was corrected for variation in the internal standards and used for statistical analyses after log2 transformation of metabolite intensities (Supplemental digital material: Appendix C). Annotation of selected apolar compounds from the LCMS analysis was performed by manually checking and matching the observed accurate mass of the putative molecular ions with available metabolite databases, including those provided by LipidMaps (http://www.lipidmaps.org) and the Human Metabolite Database (http://www.hmdb.ca), within a mass deviation of 3 ppm. Selected polar metabolites from the GCMS analysis were tentatively identified by comparing their mass spectra and/or retention index with those of authentic reference standards and of commercial and in-house electron-impact mass spectral libraries (NIST14, GolmDB). “Unknown” annotation was assigned when the mass spectra did not match reasonably with any used database. Assignation of NA (not annotated) was given for those metabolites not manually annotated, therefore automated match was not reported.

## 2.7. Statistical analysis of omics

Principal Component Analyses (PCA) of omics datasets were performed using SIMCA-P version 14.0 (MKS solutions, Umea, Sweden). Protein and transcriptome data were merged based on the gene identifiers from Phatr3 Ensembl and analysed in Perseus software [48]. Genes, proteins and metabolites that met the criterion of an FDR corrected $p$-value $< 0.05$ were considered to be significantly differentially regulated in N limited conditions in either the light or dark period. Differential expressed genes and proteins were mapped to KEGG pathways using a tool to map multiple KEGG identifiers to the pathway (MapOmics, access to the test version can be obtained from linda.bakker@wur.nl). Pathway $p$-values were calculated according to Eq. 4 where K equals the unique features known in this pathway, k for the searched features uniquely mapped on this pathway, N as the unique

features known in all pathways and n for the searched features uniquely mapped on all pathways.

$$P(X = k) = f(k, N, K, n) = \frac{\binom{K}{k}\binom{N-K}{n-k}}{\binom{N}{n}} \quad (4)$$

## 3. Results

### 3.1. Physiological response of Phaeodactylum tricornutum to nitrogen limitation

Nitrogen limitation was induced in continuous, turbidostat controlled reactors with a separate continuous nitrogen supply [42]. Turbidostat control ensures a fixed light absorption over the culture throughout the entire experiment, because the in- and out-coming light intensity are kept constant during the light period through automated dilution of the culture. The control culture was exposed to an excess of nitrogen, meaning that growth in this culture was only limited by the supplied light. The N limited cultures were exposed to a constant and limiting nitrogen supply. This turbidostat-nutristat approach allowed for simultaneous growth and lipid production [29,42]. Diurnal cycles of 16 h of light and 8 h of dark were applied to the cultures. As a consequence to the light-dark (LD) cycle, 24 h repeating diurnal oscillations in dilution rate and biomass concentration were observed. Overflow was collected on ice over 24 h hours. This overflow was used to determine the average values for the relevant physiological parameters (Table 1).

Under N replete conditions, i.e. when nitrate is not limiting, an average growth rate (i.e. dilution rate) of 0.42 ± 0.02 $day^{-1}$ and biomass concentration of 1.60 ± 0.13 g $L^{-1}$ was found, while approximately 57% of the absorbed photons were used to produce biomass (Eq. 3, Table 1 and Fig. 2B). The dry matter of N replete cells consists primarily of proteins (57% w/w), carbohydrates (13% w/w), membrane lipids (7% w/w), triacylglycerol (3% w/w) and ash (10% w/w) (Fig. 2A). Other studies found a similar biomass composition for N replete cultures of *P. tricornutum* [8,53,54], highlighting the reliability of our applied cultivation method.

When the culture was subjected to N limitation, the pigmentation (i.e. absorption cross section) visibly decreased with a consequent turbidostat-mediated increase in biomass concentration to 2.28 ± 0.10 g $L^{-1}$. Simultaneously, the specific growth rate decreased to 0.11 ± 0.02 $day^{-1}$, leading to a 3-fold decrease in both biomass productivity and yield on light for the N limited cultures as compared to the N replete cultures. Under N limitation, only 20% of the absorbed photons were used to form biomass (Eq. 3, Fig. 2B). However, the TAG productivity and TAG yield on light increased more than two-fold upon N limitation as reflected in the changed biomass composition. The relative TAG (16% w/w) and total carbohydrate (25% w/w) content increased at the expense of protein (38% w/w) and membrane lipids (5% w/w) (Fig. 2A). With our turbidostat-nutristat approach, we were able to induce TAG accumulation in continuous growing cultures under a daily repeating of LD cycles. Both conditions showed steady state oscillating patterns synchronized to the LD cycles. The oscillations were very reproducible, both between the six days of each single steady state and between the four biological replicates of each condition (e.g., N replete and limited). This allows an accurate determination of the transcriptome, proteome and metabolome in each condition on different time points of the LD cycle.

**Table 1**
Physiological parameters of continuous cultures of *P. tricornutum* under nitrogen replete and nitrogen limited growth conditions and exposed to 16:8 h LD cycles. Abbreviation: TAG, *triacylglycerol*. The values represent the mean and standard deviation of 24 h-collected culture overflow of four biological replicate experiments ($N = 4$) for each tested condition.

| Parameter | N replete | N limitation |
|---|---|---|
| Dilution rate ($day^{-1}$) | 0.42 ± 0.02 | 0.11 ± 0.02 |
| Biomass concentration (g $L^{-1}$) | 1.60 ± 0.13 | 2.28 ± 0.10 |
| Biomass productivity (g $L^{-1}$ $day^{-1}$) | 0.68 ± 0.07 | 0.25 ± 0.04 |
| Biomass yield on light (g $mol_{ph}^{-1}$) | 0.95 ± 0.09 | 0.35 ± 0.05 |
| Absorption cross section (kg $m^{-2}$) | 0.16 ± 0.02 | 0.09 ± 0.01 |
| Photosynthetic conversion efficiency (% of absorbed photons used for biomass production) | 58 ± 3 | 20 ± 1 |
| TAG content (% of dry weight) | 3 ± 1 | 16 ± 1 |
| TAG productivity (g $L^{-1}$ $day^{-1}$) | 0.02 ± 0.00 | 0.04 ± 0.01 |
| TAG yield on light (g $mol_{ph}^{-1}$) | 0.03 ± 0.01 | 0.06 ± 0.01 |

### 3.2. Physiological response to diurnal light:dark cycles

The cultures were synchronized to diurnal LD cycles (16 h of light and 8 h of dark), which resulted in differences in dilution rate (i.e. growth) throughout a daily 24 h cycle (Fig. 3). Interestingly, a clear peak in culture dilution rate, equivalent to specific growth rate due to the observed constant biomass concentration, was found around midday (i.e. 6–10 h after switching on the light) for both N replete and N limited conditions. Similar patterns were reported for continuous turbidostat cultures of *Neochloris* and *Acutodesmus* [30,55]. The biomass composition remained constant over 24 h for both treatments, except for the total carbohydrate fraction in N replete conditions, which increased significantly and specifically during the last 6 h of the light period: from 12% at $t = 10$ to 18% at $t = 16$ h of light (Fig. 3B). Similar findings for carbohydrate profiles were found in continuous N replete cultures of *Neochloris oleoabundans* [30] and *P. tricornutum* during LD cycles [53]. Both TAG and carbohydrates were significantly higher in the N limited cultures as compared to the N replete cultures, throughout the LD cycle. This result indicates that the largest differences in biomass composition were found between the treatments (N limitation versus N repletion), whereas only small or no diurnal effects were observed on biomass production.

### 3.3. Differential expression of transcripts, proteins and metabolites due to nitrogen limitation

In this study we detected in total 12,179 transcripts, 3171 proteins and 779 metabolites. As observed for the macromolecular biomass composition (Table 1 and Fig. 3), the strongest effects in the transcriptome, proteome and metabolome were related to the two nitrogen treatments (Supplementary file F). Principal component analysis (PCA) showed distinct separate clusters of the N limited samples and the N replete samples on the first principle component (PC) explaining the 28.7%, 27.8% and 54.4% of the total variance in the transcriptome, proteome and metabolome, respectively (Supplementary file F). Interestingly, only the transcriptome data showed a clear LD effect (second PC, explaining the 18.2% of the total variance): here all samples taken in the light period (5, 10, or 16 h of illumination) are separated from samples taken after the 8 h of darkness (0 h of illumination). Therefore, we focussed our further data analyses on the overall differences caused by nitrogen supply as well as the differences between dark and light (i.e. 0 versus 10 h of illumination).

Statistical analysis showed that 22% (2699) of the transcripts, 17% (543) of the proteins and 44% (345) of the metabolites in our dataset were differentially expressed under N limitation compared to the N replete conditions (n samples = 4 for both treatments, FDR corrected). These differentially expressed genes, proteins and metabolites were subsequently compared for their expression profiles in light and dark. Interestingly, the Venn diagrams (Fig. 4) indicate that most of the altered transcripts (88%) and proteins (73%) showed a diurnal regulation. The remaining 22% of the altered transcripts and 37% of the altered proteins were differentially regulated at both time points of the day, showing a response that is independent from diurnal regulation

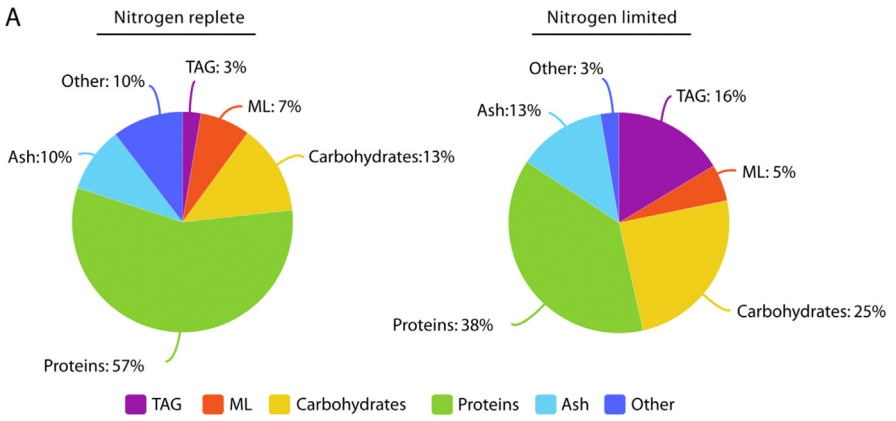


**Fig. 2.** Mass and photon distribution for nitrogen replete and nitrogen limited continuous cultures of *P. tricornutum*. A: Macromolecular biomass composition in % of dry weight (w/w) for nitrogen replete (left; control) and nitrogen limited (right) cultures. B: Photon conversion efficiency into biomass. The values were calculated using Eq. 3. Each number represents the mean of biological replicates ($N = 4$). Functional biomass consists of membrane lipids (ML), carbohydrates, proteins, triacylglycerol (TAG), ash and others. The increase in carbohydrate productivity upon nitrogen limitation is considered as additional storage carbohydrate accumulation.

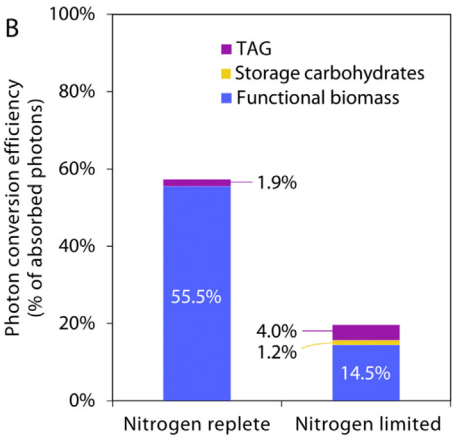


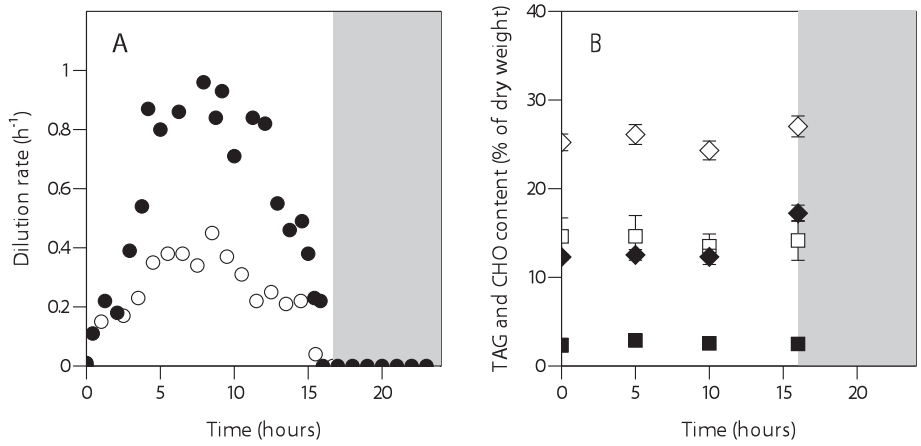


**Fig. 3.** (A) Dilution rate and (B) biomass composition (TAG and total carbohydrate [CHO]) of nitrogen replete (closed symbols) and nitrogen limited (open symbols) cultures of *P. tricornutum*. The values represent the mean of four biological replicates ($N = 4$) after 6 consecutive days of 'stable' steady state conditions. Triacylglycerol (TAG) is shown in squares and total carbohydrates (CHO) in diamonds. The shaded areas indicate the dark period.

and therefore consequent to N limitation treatment (Fig. 4). Interestingly, the metabolome showed an opposite pattern: 70% of altered metabolites were differently present at both time points and only the remaining 30% showed a diurnal regulation.

### 3.4. Cellular pathway alterations

A total of 1147 out of the 12,179 identified transcripts (9.4%) and 731 out of the 3171 identified proteins (23%) could be mapped onto KEGG pathways. Due to the limited annotation of *P. tricornutum* genome, only 340 out of the 2699 (13%) differential nitrogen-responsive transcripts and 158 out of the 543 (29%) differential nitrogen-responsive proteins could be mapped onto KEGG pathways (Fig. 5, Supplementary file G). Fig. 5 shows the effect of N depletion on the main cellular pathways. Most distinct differences occurred in pathways linked to photosynthesis, lipid, nitrogen and carbon metabolism, and amino acid degradation. Simultaneously, N limitation set constraints on the DNA replication and translation, which can be also a consequence of growth reduction.

Since the metabolomics data were primarily produced in an untargeted manner, annotation was performed manually only for a selected set of the most significantly affected compounds. KEGG identifiers could be retrieved and mapped onto KEGG pathways for only a few differentially accumulated compounds, therefore metabolomics data were not included in the pathway analysis of Fig. 5 (data in Supplementary file G).

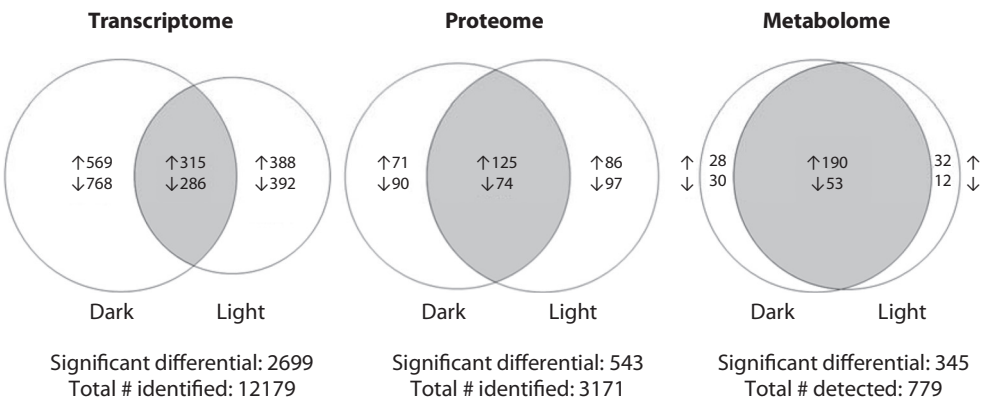


**Fig. 4.** Effect of nitrogen limitation on the number of differential expressed genes, proteins and metabolites. Differential expression was calculated by comparing the average expression values for nitrogen limited growth to nitrogen replete growth in the dark period (0, after 8 h darkness) or the light period (10, after 10 h of illumination), with $p$ value $< 0.05$. The sample set was further separated for both light and dark periods to illustrate the light-independent nitrogen-regulated differential expression (grey zone) and light-dependent nitrogen-regulated differential expression in either the dark or light period of the day. Upward arrows indicate upregulation of genes, proteins or metabolites under nitrogen limitation, whereas downwards arrows indicate downregulation under N limitation, as compared to nitrogen replete conditions.

Fig. 5 and Supplementary file H show a minor discrepancy in the regulation of transcript and proteome expression. Discrepancies between transcript and protein levels have been reported in other studies [20,56] and may be the result of a time delay between changes in gene expression and changes in protein content [57]. This time delay may be a result of post-translational regulations and/or protein turnovers.

### 3.5. Manual analysis of transcriptome and proteome

Limited by the poor annotation of *P. tricornutum* genome, we performed an additional analysis by looking at the transcripts and proteins that showed the biggest differences in expression profile during N-limited conditions compared to N-repletion. To do so, we selected only the transcripts with a log2fold change larger than 5 or smaller than −4 and the proteins with a log2fold change larger than 3 and smaller than −3. We then manually looked at their predicted domains and we made our suggestion on possible functions (Supplementary file I). In this analysis, we divided in group A the transcripts and proteins showing the highest expression levels during N-limitation compared to N-repletion, and group B the ones showing the lowest expression levels. Among the members of group A we found some of the genes related to nitrogen metabolism (Section 4.2); moreover, structural building components such as frustulin 3 (Phatr3_J51797), a glycoprotein with putative role in cell wall regeneration (Phatr3_J50390) and a coccolith scale associated

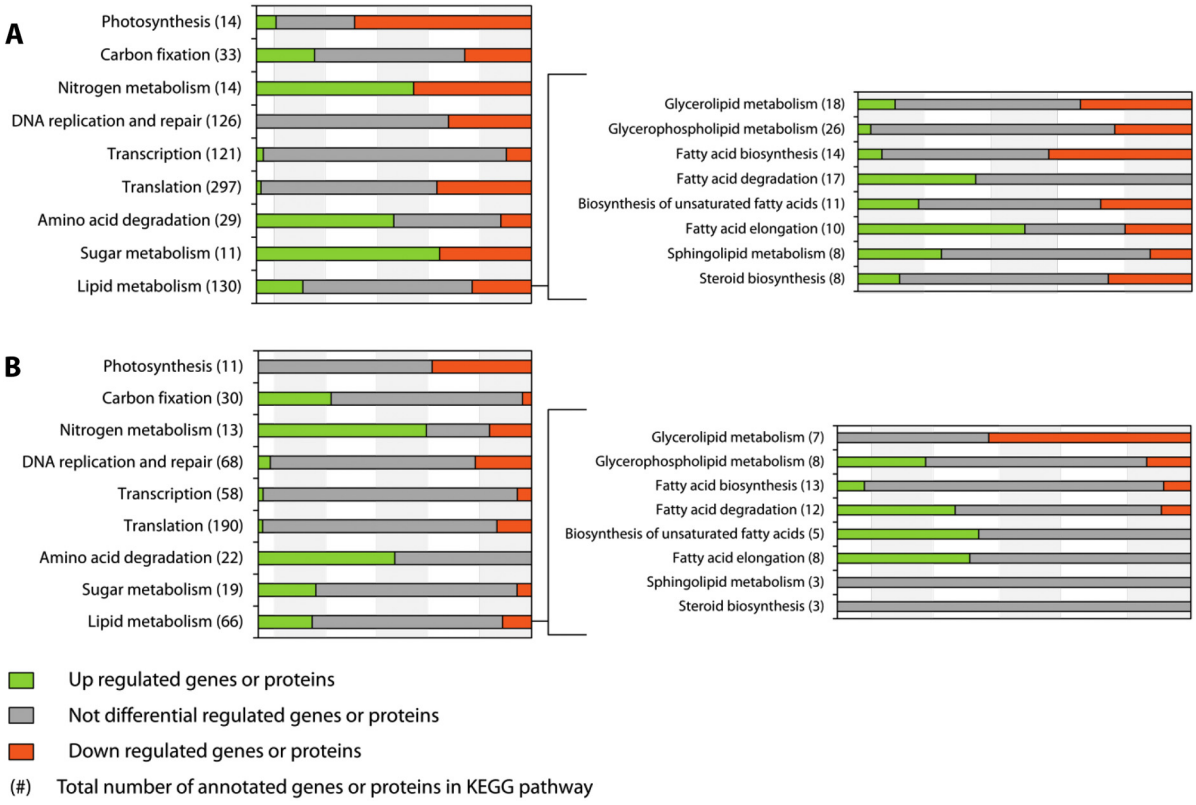


**Fig. 5.** KEGG pathway analysis for the transcript (A) and proteome (B) dataset. Colour bars indicate the percentage of genes or proteins within each pathway that are significant differentially expressed under nitrogen limited growth conditions in both light and dark period. Differential up-regulation is shown in green, no differential expression is shown in grey and differential down-regulation is shown in red. KEGG pathways are listed in random order with the total number of annotated genes or proteins in the KEGG database in brackets. (For interpretation of the references to colour in this figure legend, the reader is referred to the web version of this article.)

protein (Phatr3_J55010); the latter has been already found upregulated during nitrogen starvation in other studies and it has been suggested to be associated to lipid bodies [18,31,58,59]. We also found in group A several predicted transport channels: a protein containing sodium/dicarboxylate transporter domain (Phatr3_J50149), a CLC voltage-gated chloride channel domain containing protein (Phatr3_EG01952) and a predicted porine-like protein (Phatr3_J40228); moreover, predicted proteins that may be involved in signal transduction: 2 proteins containing Ado-Met domain (Phatr3_J49734 and Phatr3_EG02032), generally involved in methylation processes [60]; one DNA-binding domain protein (Phatr3_J49567) and one putative leucine-rich receptor-like kinase (Phatr3_J1379).

Interestingly, among the most downregulated transcripts and proteins (group B) we found genes related to redox process, such as a flavodoxin protein (Phatr3_J23658), and a putative proton-pumping pyrophosphatases (V-PPase, Phatr3_J15815), which couples the energy of pyrophosphate (PPi) hydrolysis to proton movement across membranes; member of this family are associated with roles in vacuole acidification [61]. Moreover in group B we found members of the iron stress response protein (ISIP 2A, 2B, 1, 3), which are considered to be involved in iron sensing and acquisition [28,62,63]; proteins likely involved in the xantophyll cycle and in the carotenoid metabolism: two isoforms of zeaxanthin epoxidase (ZEP1 and 2, Phatr3_J45845 and Phatr3_J5928, respectively); a zeta-carotene desaturase (ZDS, Phatr3_J9040) and a violaxanthin deepoxidase like protein (VDL, Phatr3_J36048). Finally, in group B we also found two proteins involved in glucose metabolism (Section 4.3): a triose phosphate isomerase enzyme (Phatr3_J50738) involved in gluconeogenesis and the fructose-bisphosphate aldolase isoform FABC5 (Phatr3_J41423).

## 4. Discussion

Our analysis is the result of an integrated look at the alterations in physiology, transcriptome, proteome and metabolome, which gives a comprehensive picture of the response of *P. tricornutum* to N limitation during steady state growth. Physiologically, TAG and carbohydrates were more accumulated in the N limited cultures as compared to the N replete cultures, at the expense of growth, DNA replication and protein content (Table 1 and Fig. 5). Nitrogen is an essential constituent element of several molecules, such as amino acids/proteins, nucleic acids and chlorophylls and its scarcity severely affected their associated pathways.

The reduction in cell growth during N limitation (3 fold compared to N replete conditions, Table 1) could be a result of slower cell cycle progression [64,65]. Metabolic rearrangements due to altered cell cycle progression may also have an impact on the observed results [66]; however, in our experimental conditions it is hard to decouple the reduced cell growth consequences from N limitation effects.

Overall, pathways associated to photosynthesis, N assimilation and central carbon metabolism were strongly influenced. From our results, it appeared evident that N limitation is triggering nitrogen scavenging mechanisms and, less intuitively, a change in structural building components such as cell wall and membrane lipids. Moreover, among the highest downregulated transcripts and proteins, we found several proteins related to redox processes. This may suggest that N limitation contribute to a redox imbalance inside the cell. In particular, Guerra et al. have shown an increase of NADPH/NADP+ ratio, which may contribute to an overall change in redox status of the cells under N limitation [67]. Moreover, increase of cyclic electron transport (CET) and alternative electron transport (AET) with possible consequent increase of the reduction of plastoquinone (PQ) pool have been recently reported in a photosynthetic study performed under N limitation and dynamic light conditions [68]; it is therefore plausible to suggest that N limitation may contribute to alterations in the proton/electron ratio, availability and distribution inside the cell. However, further investigations in this respect are necessary to better understand the redox status of the cells and homeostasis mechanisms during N-limitation and their implications in the cell metabolism and carbon allocation.

In our metabolome analysis we found particular high accumulation of several sugars, intermediate metabolites of the tricarboxylic acid (TCA) cycle, and changes in lipid composition (Supplemental digital material: Appendix C). Intriguingly, we also found accumulation of both acrylic acid and dimethylsulfoniopropionate (DMSP); these metabolites are usually correlated with sulfur metabolism [69–71] and DMSP has also been proposed to act as osmolyte, in substitution of proline, during N limitation [70,72]; proline indeed was found among the lowest accumulated metabolites, as well as most of the free amino acids (Supplemental digital material: Appendix C). Further investigations in this regard are needed to establish how fluid balances are regulated differently during N scarcity.

### 4.1. Impact on photosynthesis

Under nitrogen-limited turbidostat-controlled conditions, *P. tricornutum* cells are exposed to an energy imbalance between supply of light and the demand by cellular metabolism and growth. Downregulation of genes associated to photosynthesis, reduction in chlorophyll *a* and fucoxanthin content, and drop in PSII quantum yield have been extensively documented for *P. tricornutum* and other microalgae [20,73–75]. Overall, the down-regulation of biosynthesis of photosynthetic proteins likely preserves amino acid availability, especially in the case of glutamate, which is extensively used for the chlorophyll biosynthesis. In line with these findings, our transcriptome and proteome analysis showed that the majority of the genes and proteins associated to photosynthesis and chlorophyll biosynthesis are significantly downregulated under N limitation for both the dark and light period (Fig. 6).

Among them, we found significant differential expression for 19 of the 40 light harvest complex (LHC) proteins (Fig. 6). LHC proteins constitute a large family of proteins with diverse functions in both light-harvesting and photoprotection. In diatoms, LHC proteins have been divided in three main groups: the LHCFs, encoding the major fucoxanthin Chl a/c binding proteins, the red algal-like LHCRs, and the stress-responsive LI818/LHCSR-like LHCXs [76]. Moreover, a more recent evolutionary analysis showed that LHCR protein can be subdivided into two additional groups: LHCRI and LHCRII [77]. Interestingly, among all the differentially regulated LHC proteins, only LHCR 6, 8, 10 (members of LHCRII group) and LHCX4 showed upregulation; in particular, the LHCR 6 and 10 showed increased protein abundance and LHCR 8, 10, and LHCX4 showed upregulation of their transcripts at 0 h of illumination (after 8 h of darkness) during N limitation. We also saw upregulation of LHCR 12 (LHCRI group) transcript after 10 h of illumination. Nymark et al. reported a strong induction of these same LHCRII representatives (LHCR 6, 8, 10) within 30 min of exposure to light, after 48 h of dark incubation. Although the functional roles of the proteins encoded by the LHCX and LHCR-II genes are not completely elucidated yet, it has been suggested an involvement of these genes in photoprotection [77–79]. It has also been shown that an energy imbalance due to overexposure to light, also under N limited conditions, can result in photo-damage [80–82], therefore upregulation of LHCR 6, 8 and 10 and LHCX4 would be in line with the hypothesis of a photoprotection role for these proteins.

### 4.2. Nitrogen uptake and assimilation

In response to N limitation, most nitrogen metabolism-related transcripts and proteins were upregulated, suggesting a strong engagement of the cells in acquisition, remobilization and redistribution of intracellular nitrogen. Genes and proteins involved in assimilation and carrier of nitrate and ammonium were mainly upregulated, as the cells are likely trying to capture and recycle any trace of nitrogen (Fig. 7); we also showed that a considerable amount of the most expressed genes (16% of the analysed

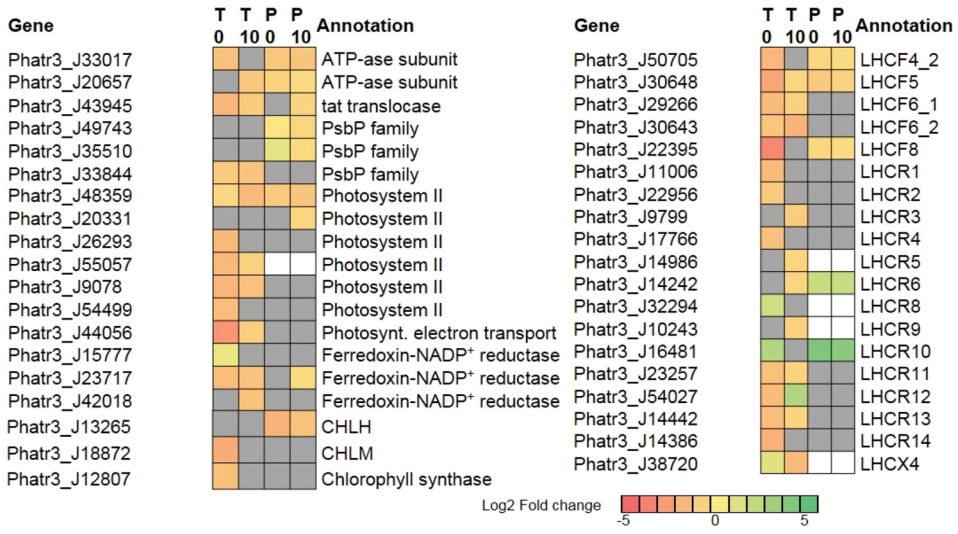


**Fig. 6.** Differential expression of photosynthesis-related genes and proteins for nitrogen limited cultures of *P. tricornutum* compared to nitrogen replete growth. The values refer to the fold change in nitrogen limited cultures in the dark period (0, after 8 h darkness) or the light period (10, after 10 h of illumination) compared to nitrogen replete cultures that were sampled at identical time points. Grey boxes represents annotated transcripts or proteins that were not significantly differentially expressed ($p$ value > 0.05). An empty box indicates that the transcript or protein was not present in the dataset. Letter abbreviations: T, transcript, P, protein. Gene abbreviations: PsbP, *photosystem II binding protein P*, CHL, *magnesium protoporphyrin IX methyltransferase* (M) and *chelatase* (H), involved in chlorophyll biosynthesis; LHC, *light harvest complex protein*. Full descriptions of the annotations, fold-changes and FDR-corrected $p$-values can be found in the Supplemental digital material: Appendix A and B.

genes in Supplementary file I) may play a role in nitrogen assimilation/scavenger mechanism. Unlike other green microalgae and plants, diatoms present an ornithine-urea cycle (OUC) that seems to facilitate rapid recovery from prolonged N limitation [83]. It has been proposed that OUC may play a crucial role in re-balancing the demand for carbon and nitrogen during fluctuating nitrogen availability [84,85]. In our metabolome, we found a significant reduction of ornithine levels and we also saw an increase in the transcript and protein of Urease C enzyme (Phatr3_J29702), which hydrolyses urea to ammonia, suggesting a direction of OUC towards ammonia assimilation. Ammonia can be assimilated into glutamate via glutamine

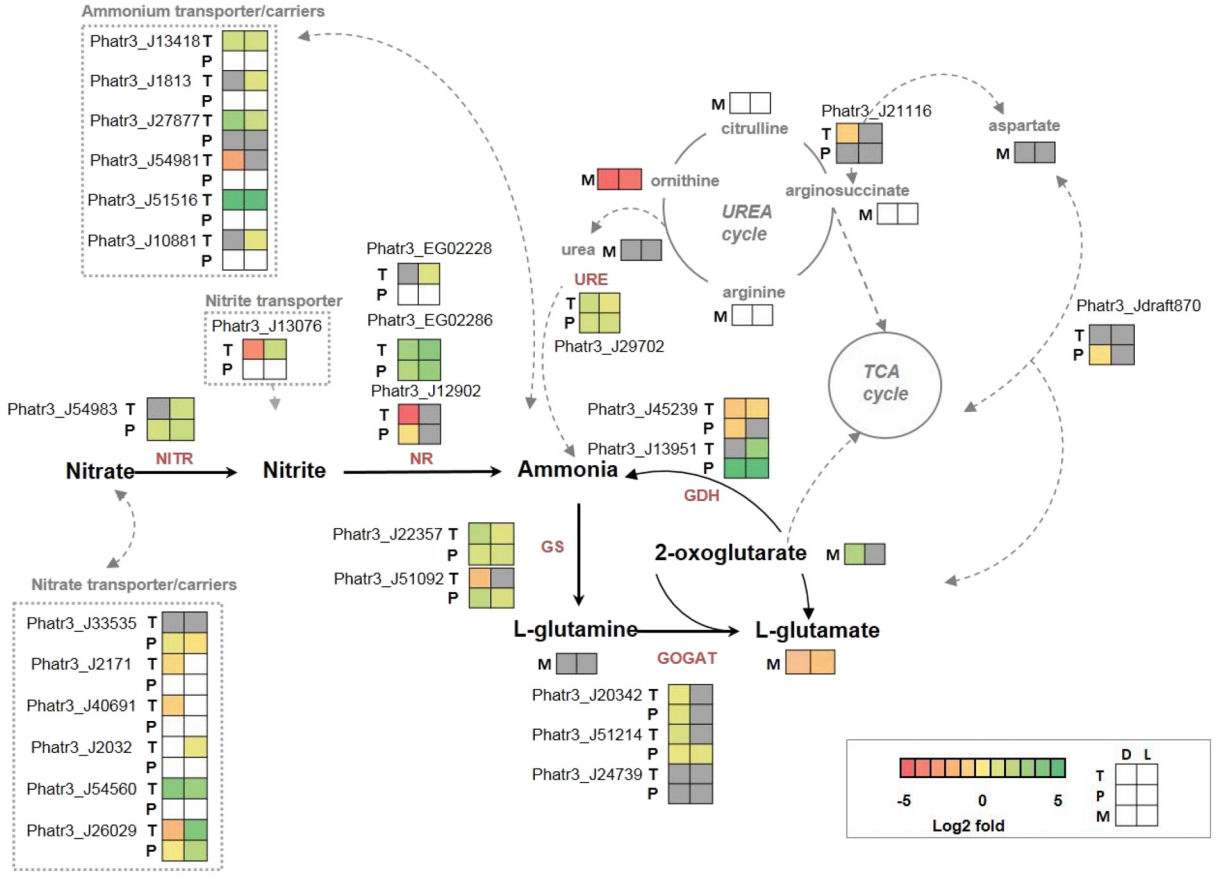


**Fig. 7.** Differential expression of nitrogen metabolism related genes (T) and proteins (P) and metabolites (M) for nitrogen limited cultures of *P. tricornutum* compared to nitrogen replete growth. The values in boxes illustrate the fold change in nitrogen limited cultures in either the dark period (D, after 8 h darkness, left box) or the light period (L, after 10 h of illumination, right box) compared to nitrogen replete cultures that were sampled at identical time points. Grey boxes represent annotated transcripts, proteins or metabolites that were not significantly differentially expressed. An empty box indicates that the transcript, protein or metabolite was not present in the dataset. Letter abbreviations: T, transcript, P, protein, M, metabolite. Enzyme abbreviations: NITR, *nitrate reductase*, NR *nitrite reductase*, GDH, *glutamate dehydrogenase*, GS, *glutamine synthase*, GOGAT, *NADPH-dependent glutamine:2-oxoglutarate amidotransferase*. Full descriptions of the annotations, fold-changes and FDR-corrected $p$-values can be found in the Supplemental digital material: Appendix A, B and C.

synthase (GS) and NADPH-dependent glutamine:2-oxoglutarate aminotransferase (GOGAT) pathway, or via glutamate dehydrogenase (GDH), which catalyses the reversible reaction L-glutamine + 2-oxoglutarate + NADPH + $H^+$ < ≥ 2 L-glutamate + $NADP^+$. As shown in Fig. 6, these enzymes involved in ammonia assimilation were upregulated.

2-oxoglutarate is an important intermediate of the mitochondrial tricarboxylic acid (TCA) cycle and we found increased level of this metabolite during N limitation (Fig. 7). These results are in line with previous metabolic flux analysis prediction that suggested a coupling between nitrogen assimilation, OUC and carbon metabolism via TCA cycle during N limitation [86]. It seems therefore plausible to confirm that N limitation leads to a scavenger mechanism which gravitates towards ammonia assimilation and that this hub is coupled to the intermediate metabolism of carbon in the TCA cycle.

### 4.3. Carbon content and carbon metabolism

Diatoms allocate organic carbon into two primary storage metabolites: the neutral lipid triacylglycerides (TAGs) and the storage polysaccharide chrysolaminarin [87,88]. Interestingly, a recent study showed that *P. tricornutum* only accumulates 4.9–6.0% of cellular carbon as chrysolaminarin during N starvation [87], suggesting that most of the sugar components are allocated in different ways; it is therefore possible that a portion of total sugars is directed to sustain the normal metabolism and a part is directed to structural lipids, as shown for other microalgae [89]. In our metabolomics analysis, we noticed an increment of several sugar compounds during N deprivation, including maltose and glucose (Supplemental digital material: Appendix C), while rearrangement and increment in glycolipid profile has been shown previously [86].

Glycolysis is a key primary pathway, as it provides substrate for energy production in the cell. In the final steps of glycolysis, glyceraldehyde 3-phosphate (G3P) is converted into pyruvate, which can be further converted into acetyl-CoA, the precursor of fatty acids. Most of the differentially expressed transcripts and proteins were upregulated under N limitation, suggesting a response to the reduction in photon conversion efficiency, and thus the direction of the carbon flux through the central carbon pathways, under N limitation (Fig. 8). By upregulation of the pathways related to the primary carbon metabolism, the cells may attempt to compensate the shortage of carbon for downstream metabolism.

The presence of multiple isoforms, which also showed opposite regulation, made difficult to analyse the regulation of the enzymes directly involved in the classic Embden–Meyerhof–Parnas glycolytic pathway (EMPP). To better elucidate the regulation of glycolysis/gluconeogenesis, we performed a manual data analysis to determine the predicted transit peptides for the several enzyme isoforms that were differentially expressed ($p$ value < 0.05) (Fig. 8). We found that among the annotated isoforms of phosphofructokinase (PKF), which converts fructose 6-phosphate to fructose-1,6-bisphosphate (catabolic pathway), one isoform (Phatr3_EG00092) with a predicted chloroplast transit peptide was downregulated during the dark phase, while the predicted cytosolic isoform (Phatr3_J14284) was upregulated. This result suggests that during the dark phase the glycolytic catabolic pathway mainly takes place in the cytosol. However, it is known that diatoms have a quite distinct carbon metabolism compared to other microalgae and higher plants [17,84,90,91]. In this respect, Fabris et al. proposed the presence of two additional and alternative carbohydrate metabolisms, the Entner–Doudoroff pathway (EDP) and the phosphoketolase pathway (PKP) [92]. In our analysis, the predicted genes involved in EDP were not differentially expressed, although we found upregulation of the transcripts and proteins of the oxidative pentose phosphate pathway (OPPP) and of the PK transcript (Phatr3_J36257), which is predicted to catalyse the conversion of xylulose-5-phosphate to acetyl-phosphate and glyceraldehyde-3-phosphate (Fig. 8). More in-depth studies on carbon allocations should be performed in order to better elucidate the involvement of any of these pathways and their contribution to lipid accumulation.

Intriguingly, we found that most of the enzyme isoforms of the lower part of the classic EMP glycolytic pathway that were differently regulated presents predicted mitochondrial transit peptides [45,93–96], suggesting that this organelle is highly engaged in the carbon allocation during N limitation (Fig. 8).

Overall, these results indicate a different involvement in carbon metabolism of the several isoforms and an orchestration among the several compartments during glycolysis and gluconeogenesis. Further studies will be required to solve this intricate thus fascinating metabolic network and regulation. Therefore our results highlight the complex fluctuations of glycolytic enzymes in the plastid and cytosol and suggest that proteins that catalyse the same reaction can have different functions and kinetics and distributes in several compartments.

### 4.4. Mitochondrion and TCA cycle may play an important role in carbon reallocation during nitrogen limitation

It is likely that cell metabolism is directed to recycle components and to use the energy and reducing power through the TCA cycle. Indeed, most of the annotated transcripts and resulting proteins associated to the TCA cycle were upregulated upon N limitation (Figure), as also previously reported [73–75].

In Fig. 5 we showed upregulation of amino acid degradation transcripts and proteins. In line with this finding, the levels of several free amino acids were significantly decreased under N limitation (Supplemental digital material: Appendix C and E). Protein synthesis, downregulation of ribosome assembly and translation are often the first and most drastic responses of cells when they experience stresses, such as nutrient limitation [20,27,28]. The differences in nitrogen metabolism and photosynthesis can be correlated to the reduced growth rate under N limitation (Table 1). Based on these observations, cell metabolism is directed to recycle components and to use the energy and reducing power through central carbon metabolism and TCA cycle, as also suggested in previous studies [66,85,86,97]. Among the TCA intermediate metabolites detected, citrate and 2-oxoglutarate showed clear and significant increased levels (Fig. 7 and Supplemental digital material: Appendix C). Citrate also serves as substrate for ATP-citrate lyase enzyme (ACL), which is considered an important player in fatty acid biosynthesis, linking the metabolism of carbohydrates (which yields citrate as an intermediate) and the production of fatty acid, by converting citrate to acetyl CoA. Interestingly, we found reduction in the transcript and protein levels for ACL, suggesting that TCA cycle is mainly engaged in recycling components to generate energy and reducing power (NADH, $FADH_2$ and GTP). Moreover, isoforms of the lower glycolytic pathway containing predicted mitochondrial transit peptide (Fig. 8) and the predicted mitochondrial pyruvate kinase (PK) were upregulated, suggesting that the resulting pyruvate is directed towards TCA cycle. Moreover, we found upregulation of predicted mitochondrial carboxylases isoforms PEPC2 and PYC1 and PYC2, enzymes designated to be involved in C4 assimilation mechanism (Fig. 9). Both enzymes produce oxaloacetate that can possibly enter directly in the TCA cycle, or that can be transported to other compartments [90].

These results suggest a pivotal role for the mitochondrion in carbon and nitrogen reallocation when the chloroplast (and photosynthesis) are affected by N limitation.

### 4.5. Effects on TAG accumulation and lipid pathway by nitrogen limitation

During N limitation, *P. tricornutum* cells accumulate lipids, mainly in the form of TAGs (Fig. 2, Supplemental digital material: Appendix C). Similarly to green microalgae, it has been proposed that TAG biosynthesis in *P. tricornutum* can occur in both chloroplast and cytosol [84,88]. In particular, the enzyme diacylglycerol O-acyltransferase (DGAT) may play a major role, being the enzyme catalysing the last

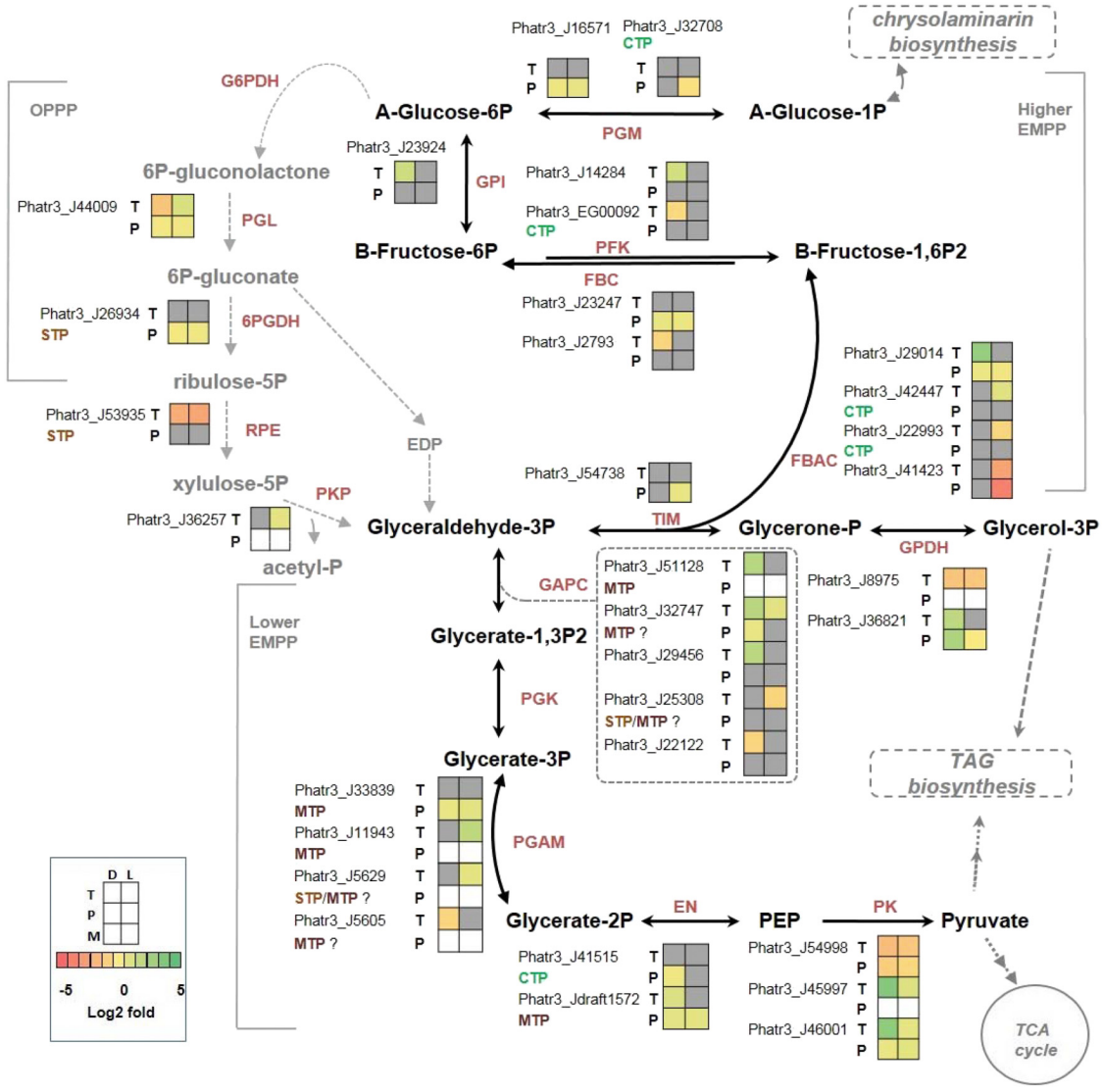


**Fig. 8.** Differential expression of central carbon metabolism related genes (T) and proteins (P) for nitrogen limited cultures of *P. tricornutum* compared to nitrogen replete growth. The values refer to the fold change in nitrogen limited cultures in the dark period (D, after 8 h darkness, left box) or the light period (L, after 10 h of illumination, right box) compared to nitrogen replete cultures that were sampled at identical time points. Grey boxes represent annotated transcripts or proteins that were not significantly differentially expressed ($p > 0.05$). Empty boxes indicate that the transcript or protein was not present in the dataset. Letter abbreviations: T, transcript, P, protein, M, metabolite. Enzyme abbreviations: PGM, *phosphoglucomutase*, GPI, *glucose phosphate isomerase*, FBC, *fructose-1,6-bisphosphatase*, PFK, *phosphofructokinase*, FBAC, *fructose-bisphosphate aldolase*, TIM, *triose-phosphate isomerase*, GPDH, *glycerol-3-phosphate dehydrogenase*, GAPC, *glyceraldehyde 3-phosphate dehydrogenase*, PGK, *phosphoglycerate kinase*, PGAM, *phosphoglycerate mutase*, EN, *enolase*, PK, *phosphoenolpyruvate kinase*, G6PDH, *glucose-6-phosphate dehydrogenase*, 6PGDH, 6-*phosphogluconate dehydrogenase*, RPE, *phosphopentose epimerase*, PK, *phosphoketolase*. Other abbreviations: PEP, *phosphoenolpyruvate*, OPPP, *oxidative pentose phosphate pathway*, EDP, *Entner–Doudoroff pathway*, EMPP, *Embden–Meyerhof–Parnas pathway*, CTP, *chloroplast transit peptide*, MTP, *mitochondrial transit peptide*, STP *signal transit peptide*. Full descriptions of the annotations, fold-changes and FDR-corrected *p*-values can be found in the Supplemental digital material: Appendix A and B.

step of TAG biosynthesis (Fig. 10); therefore, it is regarded as a promising target for improving TAG content in microalgae [98–100]. In many eukaryotes, there are two types of DGAT isoforms, DGAT1 and DGAT2. While most eukaryotic organisms contain a single copy of each DGAT isoform, photosynthetic microalgae have multiple copies of DGAT2. *P. tricornutum* contains 1 predicted isoform of DGAT1 and 4 predicted isoforms of DGAT2, named DGAT2 A, B, C, and D. Although the exact role is not elucidated yet, the overexpression of some of these isoforms in either *P. tricornutum* (Pti) or yeasts suggests a different preference for the incorporation of fatty acids into TAGs. For example, DGAT2A and DGAT2D were both overexpressed in *P. tricornutum*, leading to a 35% and 2 fold increase in TAG accumulation, respectively [15,100]. In particular, DGAT2A overexpression showed a specific increment in the portion of monosaturated fatty acids (C15:0, C17:0, C22:0) and the polyunsaturated eicosapentaenoic acid, EPA (C20:5) [15]. On the other hand, DGAT2D overexpression showed a consistent increment on fatty acid composition of C16:0, C16:1 and EPA [100].

Pti DGAT2B and DGAT1 have been characterized in yeasts, where DGAT2B showed a preference for the incorporation of the unsaturated fatty acids C16:1, C18:1 and C18:2 into the yeast TAG fraction, while DGAT1 incorporated the saturated fatty acids C16:0 and C18:0 [98,99]. In our analysis, we detected an increase of both C16:1 and C18:2 fatty acids in the TAG fraction, suggesting a possible involvement of DGAT2B during N limitation; this isoform contains a predicted chloroplast transit peptide. However, none of DGAT2 isoforms were significantly upregulated, while only the predicted DGAT1 showed upregulation at the

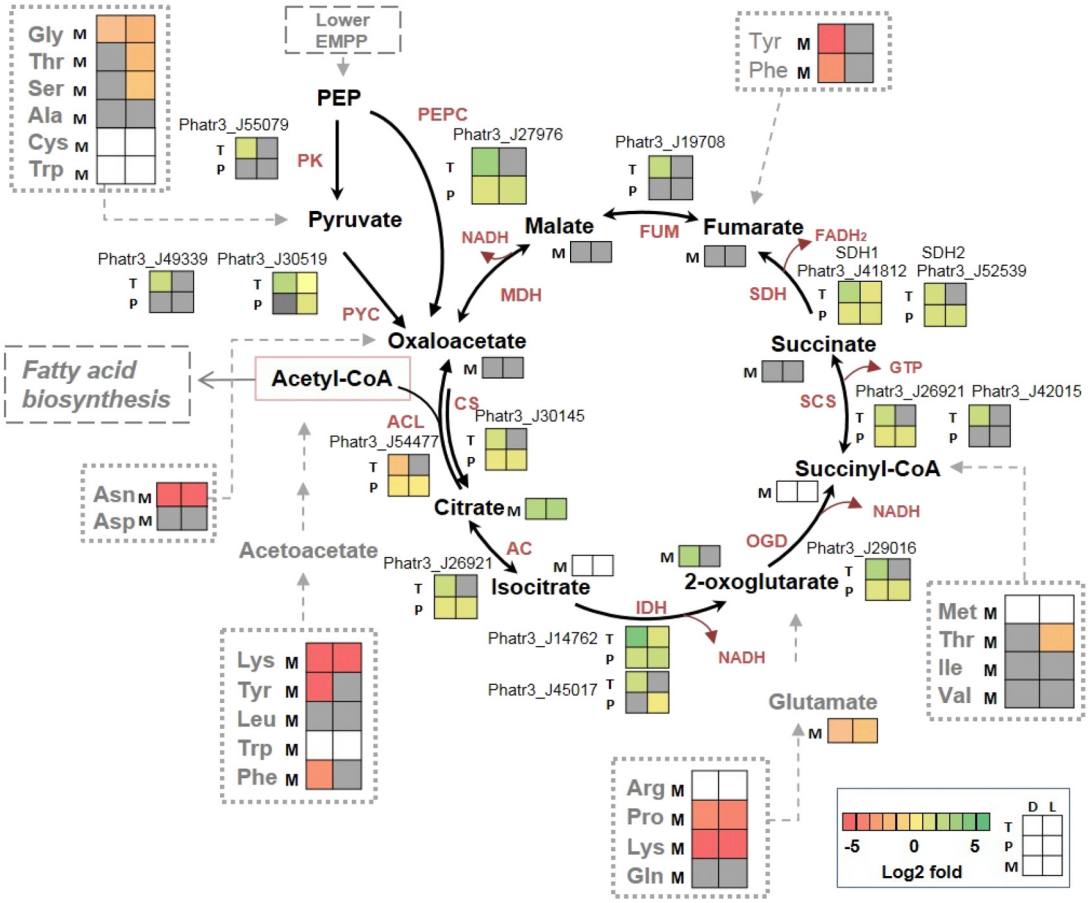


**Fig. 9.** Differential expression of the predicted mitochondrial TCA cycle related genes (T), proteins (P) and metabolites (M) for nitrogen limited cultures of *P. tricornutum* compared to nitrogen replete growth. The values refer to the fold change in nitrogen limited cultures in the dark period (D, after 8 h darkness, left box) or the light period (L, after 10 h of illumination, right box) compared to nitrogen replete cultures that were sampled at identical time points. Grey boxes represent annotated transcripts, proteins or metabolites that were not significantly differentially expressed ($p > 0.05$). Empty boxes indicate that the transcript, protein or metabolite was not present in the dataset. Letter abbreviations: T, transcript, P, protein, M, metabolite. Enzyme abbreviations: PEPC *phosphoenolpyruvate carboxylase*, PK, *phosphoenolpyruvate kinase*, PYC, *pyruvate carboxylase*, ACL, *ATP citrate lyase*, CS, *citrate synthase*, AC, *aconitase*, IDH, *isocitrate dehydrogenase*, OGD, *osoglutarate dehydrogenase*, SCS, *succinate synthase*, SDH, *succinate dehydrogenase* FUM, *fumarase*, MDH *malate dehydrogenase*. Other abbreviations: EMPP, *Embden–Meyerhof–Parnas pathway*, NADH, *nicotinamide adenine dinucleotide, reduced*, GTP, *Guanosine-5′-triphosphate*. Full descriptions of the annotations, fold-changes and FDR-corrected *p*-values can be found in the Supplemental digital material: Appendix A and B.

transcript level during the dark phase in N limited cells (Fig. 10). Further biochemical analysis will be necessary to elucidate the specific role and involvement for each of these isoforms in TAG accumulation.

Differently from other studies [20,101,102], we did not observe a significant difference in either transcript or protein expression of Acyl-CoA synthase (ACC1; Phatr3_J55209), the enzyme that catalyses the reaction from Acetyl-CoA and Malonyl-CoA to form long-chain acyl-CoA molecules. Moreover, under N limitation most of the genes involved in lipid synthesis were either downregulated or not significantly differently regulated (Fig. 10). Overall, our results suggest that DGAT activity is not a clear limiting factor during steady-state growth under N-limitation conditions, which induce TAG accumulation.

### 4.6. Membrane lipid composition suggests rearrangement towards TAG accumulation

It has also been suggested that TAG accumulation during N-starvation coincides with a reduction of membrane lipids [4,74,103]. Likewise, we observed a clear reduction of apolar metabolites related to membrane lipid metabolism, e.g., a 5-fold decrease of two phosphatidylinositol forms (38:6; total acyl carbons:total double bonds), and a 2-fold decrease of a phosphatidic acid-type of glycerophospholipid (40:4) (Supplementary digital material: Appendix C). In line with these changes in membrane lipids, membrane lipid-related pathways (glycerolipid and glycerophospholipid metabolism) were mostly down-regulated at both gene and protein expression levels (Fig. 5). Moreover, we observed a reduction of the membrane lipid content in the biomass composition of nitrogen-limited cells (Fig. 2). Similar findings have been reported, which suggested that membrane phospholipids are degraded during N-depletion to provide the TAG precursors phosphatidic acid and diacylglycerol [20,55]. This degradation may involve phospholipase C (PLC) enzyme, which selectively catalyses the hydrolysis of phospholipids by removing the phosphate head from glycerol and releasing 1,2-diacylglycerol, which can subsequently be converted into TAG by DGAT (Fig. 10). The annotated PLC enzyme (Phatr3_J42683) was not differentially regulated, while upon manually checking for genes with an annotated function in lipid processes, it appeared that 2 isoforms containing a PLC-like domain were upregulated during N-limitation (Fig. 11). Moreover, phospholipase D (PLD, Phatr3_J46400), which catalyses the production of diacylglycerol-phosphate from phosphatidylcholine and has also been proposed to be involved in the pathways for TAG production [73], was upregulated as well (Fig. 10).

Our analysis of genes with annotated functions in lipid processes also revealed at least 5 enzymes containing the alpha/beta hydrolase domain of lipases, which, interestingly, were all upregulated (Fig. 11).

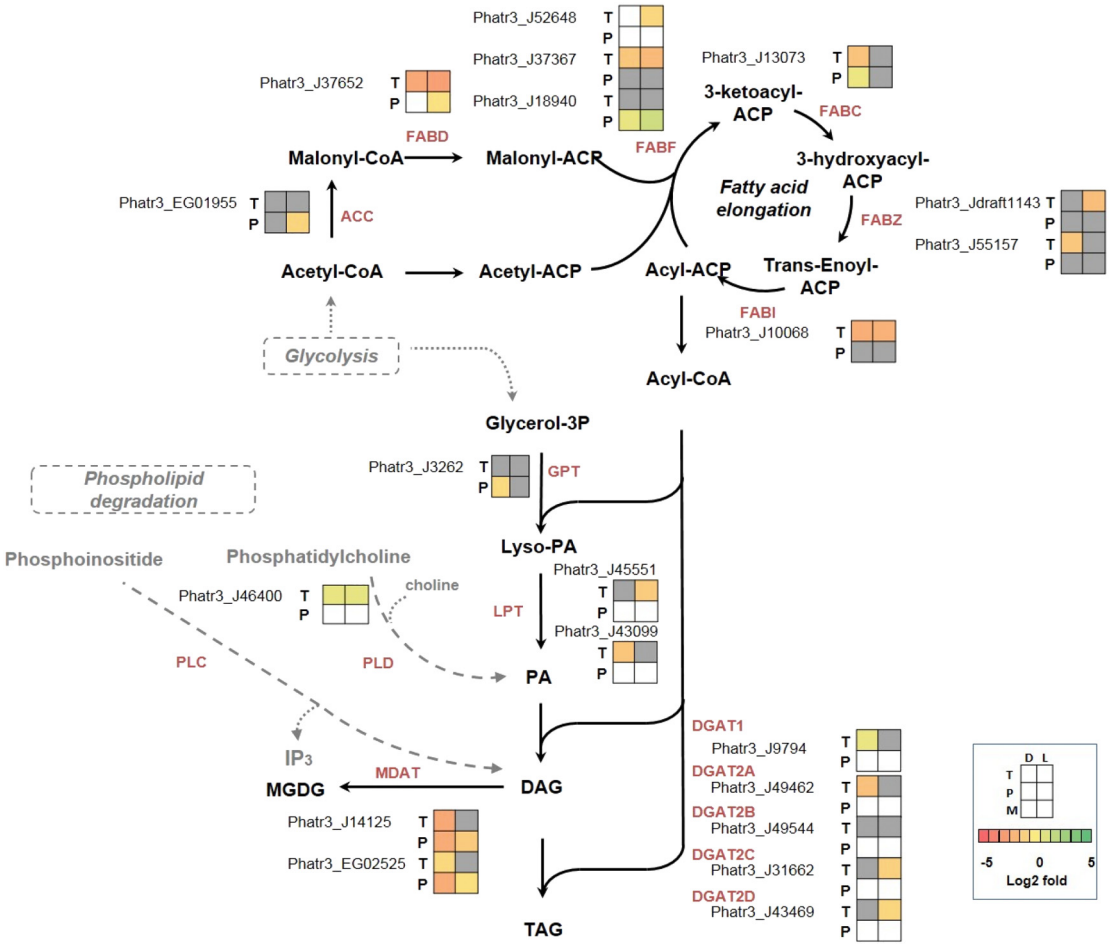


**Fig. 10.** Differential expression of genes (T) and proteins (P) involved in glycerolipid metabolism for nitrogen limited cultures of *P. tricornutum*. The values in boxes illustrate the fold change in nitrogen limited cultures in either the dark period (D, after 8 h darkness, left box) or the light period (L, after 10 h of illumination, right box) compared to nitrogen replete cultures that were sampled at identical time points. Grey boxes represent annotated transcripts or proteins that were not significantly differentially expressed ($p > 0.05$). Empty boxes indicate that the transcript or protein was not present in the dataset. Letter abbreviations: T, transcript, P, protein. Enzyme abbreviations: ACC, *acyl-CoA synthase*, FABD, *malonyl-CoA:ACP transacylase*, FABF, *3-ketoacyl-(acyl-carrier-protein) synthase II*, FABC, *acyl carrier protein*, FABZ, *3R-hydroxyacyl-[acyl carrier protein] dehydrase*, FABI, *enoyl-acp reductase*, GPT, *glycerol-3-phospate o-acyltransferase*, LPT, *1-acyl-sn-glycerol-3-phospate acyltransferase*, DGAT, *diacylglycerol o-acyltransferase*, MDAT, *monogalactosyldiacylglycerol synthase*, PLP, *phospholipase D*, PLC, *phospholipase C*. Other abbreviations: ACP, *acyl carrier protein*, PA, *phosphatidic acid*, DAG, *diacylglycerol*, TAG, *triacylgliceride*, MGDG, *monogalactosyldiacylglycerol*, IP3, *inositol-3-phosphate*. Full descriptions of the annotations, fold-changes and FDR-corrected *p*-values can be found in the Supplemental digital material: Appendix A and B.

Moreover a predicted protein (Phatr3_EG01099), containing the same lipase domain was found among the highest expressed transcripts and proteins (Supplementary file I). These findings suggest an important role of these putative lipases in lipid rearrangement towards TAG distribution and accumulation.

A significant difference in the saturation level of membrane lipids was also observed (GC-FID analysis, Supplementary file E) and transcripts for the desaturase enzymes Δ9 (Phatr3_J28797) and Δ6 (Phatr3_J29488) were upregulated (Fig. 11). Moreover, the profiling of apolar compounds of our metabolome (Supplemental digital material: Appendix C) indicated an increase of a large variety of TAG species differing in either the number of carbons and unsaturated bonds (identified by their differences in elemental formulae) or the position of carbon chains and C=C bonds (identified by their different retention times). These findings are in line with a previous study of the metabolome of *P. tricornutum* conducted by Popko et al., which suggested that betaine lipids serve as precursors for TAG formation [70]. Betaine lipids, such as diacylglyceryl-hydroxymethyl-*N*,*N*,*N*-trimethyl-beta-alanine (DGTA) and diacylglyceryl-hydroxymethyl-*N*,*N*,*N*-trimethyl-homoserine (DGTS) are found in the membranes of several microalgae and plants and they are structural similar to membrane phospholipids [70,88].

Overall, these results suggest that cells are engaged in a substantial fatty acid rearrangement, which may also be a key factor to the observed TAG accumulation (Fig. 11).

Finally, in our metabolome we found high abundance of hydroxylated eicosapentaenoic acid (EPA), as free fatty acid; we hypothesize that the hydroxylation could be a result of lipase activities (Supplemental digital material: Appendix C). However, further work on elucidating PL and lipase enzymes and their function are necessary to better understand the membrane lipid rearrangement and TAG production, possibly open novel biotechnological routes for TAG improvement.

## 5. Conclusion

Despite the extensive research on lipid production in microalgae, it is still not known which molecular mechanism(s) drives TAG accumulation during N deprivation. This study focussed, for the first time, on the combined analysis of transcriptome, proteome and metabolome of the diatom *P. tricornutum*, cultivated in high-controlled parameter photobioreactors, under N limitation conditions and light/dark cycles. Although N limitation was responsible for the major differences in transcripts, proteins and metabolites, we also observed substantial

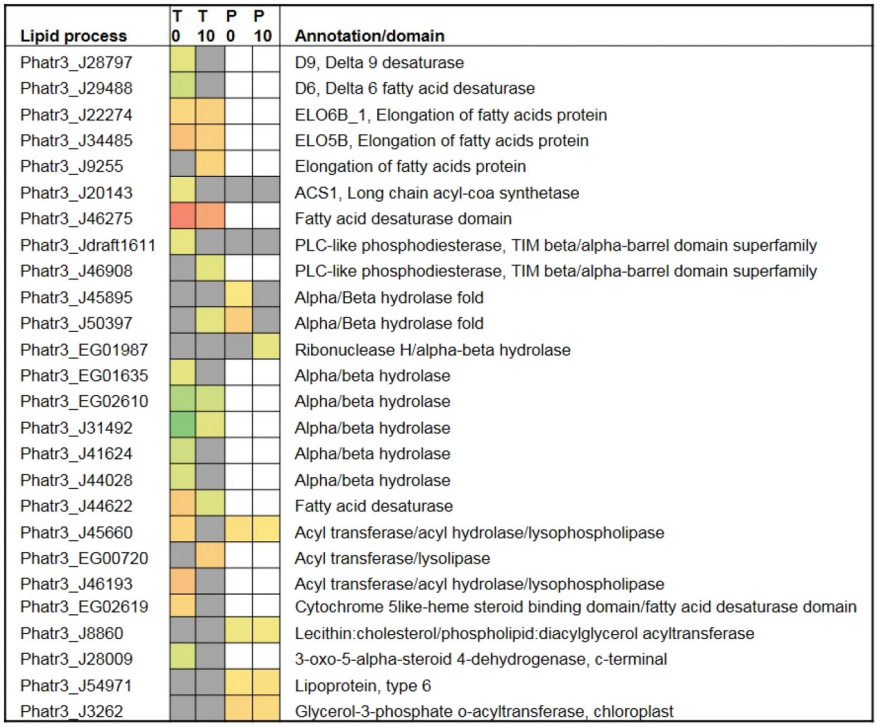


**Fig. 11.** Differential expression of genes (T) and proteins (P) involved in lipid process for nitrogen limited cultures of *P. tricornutum*. The values in boxes illustrate the fold change in nitrogen limited cultures in either the dark period (0, after 8 h darkness) or the light period (10, after 10 h of illumination) compared to nitrogen replete cultures that were sampled at identical time points. Grey box represents annotated transcripts or proteins that were not significantly differentially expressed ($p$ value > 0.05). PLC, *phospholipase C*; ELO, *elongase*. An empty box indicates that the transcript or protein was not present in the dataset. Full descriptions of the annotations, fold-changes and FDR-corrected $p$-values can be found in the Supplemental digital material: Appendix A and B.

differential gene expression, over diurnal cycle (light/dark cycles), while the proteome and metabolome were less affected.

Overall, this comprehensive -omics study shows that N limitation in *P. tricornutum* affects growth rate, photosynthesis, ribosomal and protein synthesis; on the other hand, pathways involved in nitrogen assimilation, amino acid degradation and central carbon metabolism were mainly upregulated, pointing towards an increased mitochondrial activity and TCA cycle.

We also reported a reduction of apolar metabolites related to membrane lipid metabolism and downregulation of membrane lipid-related pathways (glycerolipid and glycerophospholipid metabolism), while upregulation of genes possibly involved in rearrangements of membranes and cell wall was observed (Fig. 11 and Supplementary file I). These findings suggest that membrane rearrangements may contribute to TAG distribution.

From a biotechnological point of view, more investigations are required to elucidate which pathways, enzymes and isoform(s) would be the best targets for increasing TAG productivity. In this regard, a more in-depth investigation on DGAT and lipase enzymes, activity and selectivity, may help to unveil TAG formation and accumulation.

On the other hand, overexpression of the entire acyl-CoA – fatty acid pathway may also assist in increasing TAG productivity, as the whole pathway is currently downregulated. In addition, TAG biosynthesis is limited by the reduced carbon flux through central metabolism. Because N limitation resulted in a 5–6 fold increase in TAG content, but with a concomitant loss in growth rate and photosynthetic efficiency, and possible redox imbalance, future strain improvement should therefore not only focus on lipid metabolism, but also on improving and understanding the regulation of carbon fluxes through the central carbon metabolism, cell cycles and associated metabolism, mitochondrial activity and its involvement in sustaining the cellular metabolism, and culturing conditions.

## Acknowledgements

The authors would like to thank Benjamin von Kleist-Retzow and Nur Sabrina Binti Mohamed Zaini for their valuable input in setting up the experiments. Bert Schipper, Jeroen van Arkel and Henriëtte van Eekelen (Bioscience, Wageningen University and Research) are acknowledged for their excellent help in the metabolomics part. We thank Ron Wehrens for his help with the statistical analyses. We thank Thamara Hesselink and Bas te Lintel Hekkert from Bioscience, Wageningen University and Research for their help in the construction and sequencing of RNAseq libraries.

We also acknowledge Pacific Northwest National Laboratory for providing access to their Venn diagram drawing software (https://omics.pnl.gov/software/venn-diagram-plotter).

## Statement of informed consent

No conflicts, informed consent, human or animal rights applicable.

## Conflict of interest

Authors have no competing interests.

## Funding

This work was carried out within the EU project Fuel4Me, funded by the European Union's Seventh Programme for Research and Technology Development (EU-FP7) under grant agreement No. 308983.

## Author contributions

IR, DM, RV, RM, AA, JH, LB, SP, RW and PL conceived the research and designed the experiments; IR performed the experiments; IR, SD, RV, RM, AA, JH and LB analysed and interpreted the data; IR and SD wrote the article. SD, DM, RV, AA, JH, LB, SP, RW and PL edited the manuscript; All authors read and approved the final manuscript.

## Supplementary data

Supplementary data to this article can be found online at https://doi.org/10.1016/j.algal.2018.08.012.

## References


[1] M.S. Chauton, Y. Olsen, O. Vadstein, Biomass production from the microalga *Phaeodactylum tricornutum*: nutrient stress and chemical composition in exponential fed-batch cultures, Biomass Bioenergy 58 (2013) 87–94, https://doi.org/10.1016/j.biombioe.2013.10.004.

[2] R.B. Draaisma, R.H. Wijffels, P.M.E. Slegers, L.B. Brentner, A. Roy, M.J. Barbosa, Food commodities from microalgae, Curr. Opin. Biotechnol. 24 (2013) 169–177, https://doi.org/10.1016/j.copbio.2012.09.012.

[3] R.H. Wijffels, M.J. Barbosa, M.H.M. Eppink, Microalgae for the production of bulk chemicals and biofuels, Biofuels Bioprod. Biorefin. 4 (2010) 287–295, https://doi.org/10.1002/bbb.215.

[4] H. Abida, L.-J. Dolch, C. Meï, V. Villanova, M. Conte, M.A. Block, G. Finazzi, O. Bastien, L. Tirichine, C. Bowler, F. Rébeillé, D. Petroutsos, J. Jouhet, E. Maréchal, Membrane glycerolipid remodeling triggered by nitrogen and phosphorus starvation in *Phaeodactylum tricornutum*, Plant Physiol. 167 (2015) 118–136, https://doi.org/10.1104/pp.114.252395.

[5] T. Adarme-Vega, D.K.Y. Lim, M. Timmins, F. Vernen, Y. Li, P.M. Schenk, Microalgal biofactories: a promising approach towards sustainable omega-3 fatty acid production, Microb. Cell Factories 11 (2012) 96, https://doi.org/10.1186/1475-2859-11-96.

[6] M. Sprague, J. Walton, P.J. Campbell, F. Strachan, J.R. Dick, J.G. Bell, Replacement of fish oil with a DHA-rich algal meal derived from *Schizochytrium sp.* on the fatty acid and persistent organic pollutant levels in diets and flesh of Atlantic salmon (*Salmo salar*, L.) post-smolts, Food Chem. 185 (2015) 413–421, https://doi.org/10.1016/j.foodchem.2015.03.150.

[7] DSM, DSM Nutritional Products and Evonik Nutrition & Care to Develop Algae-Based Omega-3 Fatty Acids for Animal Nutrition, (2015) (Kaiseraugst (CH)/Essen (DE)).

[8] G. Breuer, P.P. Lamers, D.E. Martens, R.B. Draaisma, R.H. Wijffels, The impact of nitrogen starvation on the dynamics of triacylglycerol accumulation in nine microalgae strains, Bioresour. Technol. 124 (2012) 217–226, https://doi.org/10.1016/j.biortech.2012.08.003.

[9] L. Rodolfi, G. Chini Zittelli, N. Bassi, G. Padovani, N. Biondi, G. Bonini, M.R. Tredici, Microalgae for oil: strain selection, induction of lipid synthesis and outdoor mass cultivation in a low-cost photobioreactor, Biotechnol. Bioeng. 102 (2009) 100–112, https://doi.org/10.1002/bit.22033.

[10] J. Ruiz, G. Olivieri, J. de Vree, R. Bosma, P. Willems, J.H. Reith, M.H.M. Eppink, D.M.M. Kleinegris, R.H. Wijffels, M.J. Barbosa, Towards Industrial Products from Microalgae, 9 (2016), pp. 3036–3043, https://doi.org/10.1039/C6EE01493C.

[11] G. Benvenuti, R. Bosma, M. Cuaresma, M. Janssen, M.J. Barbosa, R.H. Wijffels, Selecting microalgae with high lipid productivity and photosynthetic activity under nitrogen starvation, J. Appl. Phycol. 27 (2014) 1425–1431, https://doi.org/10.1007/s10811-014-0470-8.

[12] M.J. Griffiths, R.P. van Hille, S.T.L. Harrison, Lipid productivity, settling potential and fatty acid profile of 11 microalgal species grown under nitrogen replete and limited conditions, J. Appl. Phycol. 24 (2011) 989–1001, https://doi.org/10.1007/s10811-011-9723-y.

[13] T.G. Dunahay, E.E. Jarvis, P.G. Roessler, Genetic transformation of the diatoms *Cyclotella cryptica* and *Navicula saprophila*, J. Phycol. 31 (1995) 1004–1012, https://doi.org/10.1111/j.0022-3646.1995.01004.x.

[14] Y. Li, D. Han, G. Hu, D. Dauvillee, M. Sommerfeld, S. Ball, Q. Hu, *Chlamydomonas* starchless mutant defective in ADP-glucose pyrophosphorylase hyper-accumulates triacylglycerol, Metab. Eng. 12 (2010) 387–391, https://doi.org/10.1016/j.ymben.2010.02.002.

[15] Y.-F. Niu, M.-H. Zhang, D.-W. Li, W.-D. Yang, J.-S. Liu, W.-B. Bai, H.-Y. Li, Improvement of neutral lipid and polyunsaturated fatty acid biosynthesis by overexpressing a type 2 diacylglycerol acyltransferase in marine diatom *Phaeodactylum tricornutum*, Mar. Drugs 11 (2013) 4558–4569, https://doi.org/10.3390/md11114558.

[16] V.H. Work, R. Radakovits, R.E. Jinkerson, J.E. Meuser, L.G. Elliott, D.J. Vinyard, L.M.L. Laurens, G.C. Dismukes, M.C. Posewitz, Increased lipid accumulation in the *Chlamydomonas reinhardtii* sta7-10 starchless isoamylase mutant and increased carbohydrate synthesis in complemented strains, Eukaryot. Cell 9 (2010) 1251–1261, https://doi.org/10.1128/EC.00075-10.

[17] M.A. Bromke, J.S. Sabir, F.A. Alfassi, N.H. Hajarah, S.A. Kabli, A.L. Al-Malki, M.P. Ashworth, M. Méret, R.K. Jansen, L. Willmitzer, Metabolomic profiling of 13 diatom cultures and their adaptation to nitrate-limited growth conditions, PLoS One 10 (2015) e0138965, , https://doi.org/10.1371/journal.pone.0138965.

[18] M. Garnier, G. Carrier, H. Rogniaux, E. Nicolau, G. Bougaran, B. Saint-Jean, J.P. Cadoret, Comparative proteomics reveals proteins impacted by nitrogen deprivation in wild-type and high lipid-accumulating mutant strains of *Tisochrysis lutea*, J. Proteome 105 (2014) 107–120, https://doi.org/10.1016/j.jprot.2014.02.022.

[19] S.-H. Ho, A. Nakanishi, X. Ye, J.-S. Chang, C.-Y. Chen, T. Hasunuma, A. Kondo, Dynamic metabolic profiling of the marine microalga *Chlamydomonas* sp. JSC4 and enhancing its oil production by optimizing light intensity, Biotechnol. Biofuels 8 (48) (2015), https://doi.org/10.1186/s13068-015-0226-y.

[20] J. Longworth, D. Wu, M. Huete-Ortega, P.C. Wright, S. Vaidyanathan, Proteome response of *Phaeodactylum tricornutum*, during lipid accumulation induced by nitrogen depletion, Algal Res. 18 (2016) 213–224, https://doi.org/10.1016/j.algal.2016.06.015.

[21] Z.T. Muhseen, Q. Xiong, Z. Chen, F. Ge, Proteomics studies on stress responses in diatoms, Proteomics (2015), https://doi.org/10.1002/pmic.201500165.

[22] R. Willamme, Z. Alsafra, R. Arumugam, G. Eppe, F. Remacle, R.D. Levine, C. Remacle, Metabolomic analysis of the green microalga *Chlamydomonas reinhardtii* cultivated under day/night conditions, J. Biotechnol. 215 (2015) 20–26, https://doi.org/10.1016/j.jbiotec.2015.04.013.

[23] L. Nie, G. Wu, D.E. Culley, J.C.M. Scholten, W. Zhang, Integrative analysis of transcriptomic and proteomic data: challenges, solutions and applications, Crit. Rev. Biotechnol. 27 (2007) 63–75, https://doi.org/10.1080/07388550701334212.

[24] W. Zhang, F. Li, L. Nie, Integrating multiple 'omics' analysis for microbial biology: application and methodologies, Microbiology 156 (2010) 287–301, https://doi.org/10.1099/mic.0.034793-0.

[25] S.T. Dyhrman, B.D. Jenkins, T.A. Rynearson, M.A. Saito, M.L. Mercier, H. Alexander, L.P. Whitney, A. Drzewianowski, V.V. Bulygin, E.M. Bertrand, Z. Wu, C. Benitez-Nelson, A. Heithoff, The transcriptome and proteome of the diatom *Thalassiosira pseudonana* reveal a diverse phosphorus stress response, PLoS One 7 (2012) e33768, , https://doi.org/10.1371/journal.pone.0033768.

[26] M.T. Guarnieri, A. Nag, S.L. Smolinski, A. Darzins, M. Seibert, P.T. Pienkos, Examination of triacylglycerol biosynthetic pathways via *de novo* transcriptomic and proteomic analyses in an unsequenced microalga, PLoS One 6 (2011) e25851, , https://doi.org/10.1371/journal.pone.0025851.

[27] S. Schmollinger, T. Mühlhaus, N.R. Boyle, I.K. Blaby, D. Casero, T. Mettler, J.L. Moseley, J. Kropat, F. Sommer, D. Strenkert, D. Hemme, M. Pellegrini, A.R. Grossman, M. Stitt, M. Schroda, S.S. Merchant, Nitrogen-sparing mechanisms in *Chlamydomonas* affect the transcriptome, the proteome, and photosynthetic metabolism, Plant Cell 26 (2014) 1410–1435, https://doi.org/10.1105/tpc.113.122523.

[28] S.R. Smith, J.T.F. Gillard, A.B. Kustka, J.P. McCrow, J.H. Badger, H. Zheng, A.M. New, C.L. Dupont, T. Obata, A.R. Fernie, A.E. Allen, Transcriptional orchestration of the global cellular response of a model pennate diatom to diel light cycling under iron limitation, PLoS Genet. 12 (2016) e1006490, , https://doi.org/10.1371/journal.pgen.1006490.

[29] A.J. Klok, D.E. Martens, R.H. Wijffels, P.P. Lamers, Simultaneous growth and neutral lipid accumulation in microalgae, Bioresour. Technol. 134 (2013) 233–243.

[30] L. de Winter, L.W. Schepers, M. Cuaresma, M.J. Barbosa, D.E. Martens, R.H. Wijffels, Circadian rhythms in the cell cycle and biomass composition of *Neochloris oleoabundans* under nitrogen limitation, J. Biotechnol. 187 (2014) 25–33, https://doi.org/10.1016/j.jbiotec.2014.07.016.

[31] J. Valenzuela, A. Mazurie, R.P. Carlson, R. Gerlach, K.E. Cooksey, B.M. Peyton, M.W. Fields, Potential Role of Multiple Carbon Fixation Pathways During Lipid Accumulation in *Phaeodactylum tricornutum*, (2012).

[32] L. Rodolfi, N. Biondi, A. Guccione, N. Bassi, M. D'Ottavio, G. Arganaraz, M.R. Tredici, Oil and eicosapentaenoic acid production by the diatom *Phaeodactylum tricornutum* cultivated outdoors in Green Wall Panel (GWP®) reactors, Biotechnol. Bioeng. 114 (2017) 2204–2210, https://doi.org/10.1002/bit.26353.

[33] C. Bowler, et al., The *Phaeodactylum* genome reveals the evolutionary history of diatom genomes, Nature 456 (2008) 239–244, https://doi.org/10.1038/nature07410.

[34] F. Daboussi, S. Leduc, A. Maréchal, G. Dubois, V. Guyot, C. Perez-Michaut, A. Amato, A. Falciatore, A. Juillerat, M. Beurdeley, D.F. Voytas, L. Cavarec, P. Duchateau, Genome engineering empowers the diatom *Phaeodactylum tricornutum* for biotechnology, Nat. Commun. 5 (2014) 3831, https://doi.org/10.1038/ncomms4831.

[35] V. De Riso, R. Raniello, F. Maumus, A. Rogato, C. Bowler, A. Falciatore, Gene silencing in the marine diatom *Phaeodactylum tricornutum*, Nucleic Acids Res. 37 (2009), https://doi.org/10.1093/nar/gkp448.

[36] U. Eilers, A. Bikoulis, J. Breitenbach, C. Büchel, G. Sandmann, Limitations in the biosynthesis of fucoxanthin as targets for genetic engineering in *Phaeodactylum tricornutum*, J. Appl. Phycol. 28 (2016) 123–129.

[37] M.L. Hamilton, R.P. Haslam, J.A. Napier, O. Sayanova, Metabolic engineering of *Phaeodactylum tricornutum* for the enhanced accumulation of omega-3 long chain polyunsaturated fatty acids, Metab. Eng. 22 (2014) 3–9, https://doi.org/10.1016/j.ymben.2013.12.003.

[38] M. Nymark, A.K. Sharma, T. Sparstad, A.M. Bones, P. Winge, A CRISPR/Cas9 system adapted for gene editing in marine algae, Sci. Rep. 6 (2016) 24951, https://doi.org/10.1038/srep24951.

[39] S. Seo, H. Jeon, S. Hwang, E. Jin, K.S. Chang, Development of a new constitutive expression system for the transformation of the diatom *Phaeodactylum tricornutum*, Algal Res. 11 (2015) 50–54, https://doi.org/10.1016/j.algal.2015.05.012.

[40] G. Dubois, C. Perez-Michaut, A. Amato, A. Falciatore, A. Juillerat, M. Beurdeley, D.F. Voytas, L. Cavarec, P. Duchateau, *Phaeodactylum tricornutum* for Biotechnology, (2014), pp. 1–7, https://doi.org/10.1038/ncomms4831.

[41] S. D'Adamo, G. Schiano di Visconte, G. Lowe, J. Szaub-Newton, T. Beacham, A. Landels, M.J. Allen, A. Spicer, M. Matthijs, Engineering the unicellular alga *Phaeodactylum tricornutum* for high-value plant triterpenoid production, Plant Biotechnol. J. (2018) 0–2, https://doi.org/10.1111/pbi.12948.

[42] I.M. Remmers, A. Hidalgo-Ulloa, B.P. Brandt, W.A.C. Evers, R.H. Wijffels, P.P. Lamers, Continuous versus batch production of lipids in the microalgae *Acutodesmus obliquus*, Bioresour. Technol. (2017), https://doi.org/10.1016/j.biortech.2017.04.093.

[43] G. Breuer, P.P. Lamers, M. Janssen, R.H. Wijffels, D.E. Martens, Opportunities to improve the areal oil productivity of microalgae, Bioresour. Technol. 186 (2015) 294–302, https://doi.org/10.1016/j.biortech.2015.03.085.

[44] A.M.J. Kliphuis, A.J. Klok, D.E. Martens, P.P. Lamers, M. Akedo, R.H. Wijffels, Metabolic modeling of *Chlamydomonas reinhardtii:* energy requirements for photoautotrophic growth and maintenance, J. Appl. Phycol. 24 (2012) 253–266,

https://doi.org/10.1007/s10811-011-9674-3.
[45] J. Kim, M. Fabris, G. Baart, M.K. Kim, A. Goossens, W. Vyverman, P.G. Falkowski, D.S. Lun, Flux balance analysis of primary metabolism in the diatom *Phaeodactylum tricornutum*, Plant J. 85 (2016) 161–176, https://doi.org/10.1111/tpj.13081.
[46] J. Cox, M. Mann, MaxQuant enables high peptide identification rates, individualized p.p.b.-range mass accuracies and proteome-wide protein quantification, Nat. Biotechnol. 26 (2008) 1367–1372, https://doi.org/10.1038/nbt.1511.
[47] J. Cox, M.Y. Hein, C.A. Luber, I. Paron, N. Nagaraj, M. Mann, Accurate proteome-wide label-free quantification by delayed normalization and maximal peptide ratio extraction, termed MaxLFQ, Mol. Cell Proteomics 13 (2014) 2513–2526, https://doi.org/10.1074/mcp.M113.031591.
[48] S. Tyanova, T. Temu, A. Carlson, P. Sinitcyn, M. Mann, J. Cox, Visualization of LC-MS/MS proteomics data in MaxQuant, Proteomics 15 (2015) 1453–1456, https://doi.org/10.1002/pmic.201400449.
[49] N. Carreno-Quintero, A. Acharjee, C. Maliepaard, C.W.B. Bachem, R. Mumm, H. Bouwmeester, R.G.F. Visser, J.J.B. Keurentjes, Untargeted metabolic quantitative trait loci analyses reveal a relationship between primary metabolism and potato tuber quality1[W][OA], Plant Physiol. 158 (2012) 1306–1318, https://doi.org/10.1104/pp.111.188441.
[50] J.J.J. van der Hooft, J. Vervoort, R.J. Bino, R.C.H. de Vos, Spectral trees as a robust annotation tool in LC–MS based metabolomics, Metabolomics 8 (2012) 691–703, https://doi.org/10.1007/s11306-011-0363-7.
[51] A. Lommen, H.J. Kools, MetAlign 3.0: performance enhancement by efficient use of advances in computer hardware, Metabolomics 8 (2012) 719–726, https://doi.org/10.1007/s11306-011-0369-1.
[52] Y.M. Tikunov, S. Laptenok, R.D. Hall, A. Bovy, R.C.H. de Vos, MSClust: a tool for unsupervised mass spectra extraction of chromatography-mass spectrometry ion-wise aligned data, Metabolomics 8 (2012) 714–718, https://doi.org/10.1007/s11306-011-0368-2.
[53] M.S. Chauton, P. Winge, T. Brembu, O. Vadstein, A.M. Bones, Gene regulation of carbon fixation, storage, and utilization in the diatom *Phaeodactylum tricornutum* acclimated to light/dark cycles, Plant Physiol. 161 (2013) 1034–1048, https://doi.org/10.1104/pp.112.206177.
[54] A.S. Mirón, M.C.C. Garcıa, A.C. Gómez, F.G. Camacho, E.M. Grima, Y. Chisti, Shear stress tolerance and biochemical characterization of *Phaeodactylum tricornutum* in quasi steady-state continuous culture in outdoor photobioreactors, Biochem. Eng. J. 16 (2003) 287–297, https://doi.org/10.1016/S1369-703X(03)00072-X.
[55] G.M. León-Saiki, I.M. Remmers, D.E. Martens, P.P. Lamers, R.H. Wijffels, D. van der Veen, The role of starch as transient energy buffer in synchronized microalgal growth in *Acutodesmus obliquus*, Algal Res. 25 (2017) 160–167, https://doi.org/10.1016/j.algal.2017.05.018.
[56] S. Rogers, M. Girolami, W. Kolch, K.M. Waters, T. Liu, B. Thrall, H.S. Wiley, Investigating the correspondence between transcriptomic and proteomic expression profiles using coupled cluster models, Bioinformatics 24 (2008) 2894–2900, https://doi.org/10.1093/bioinformatics/btn553.
[57] J.R. Waldbauer, S. Rodrigue, M.L. Coleman, S.W. Chisholm, Transcriptome and proteome dynamics of a light-dark synchronized bacterial cell cycle, PLoS One 7 (2012) e43432, , https://doi.org/10.1371/journal.pone.0043432.
[58] Q. Shi, H. Araie, R.K. Bakku, Y. Fukao, R. Rakwal, I. Suzuki, Y. Shiraiwa, Proteomic analysis of lipid body from the alkenone-producing marine haptophyte alga *Tisochrysis lutea*, Proteomics 15 (2015) 4145–4158, https://doi.org/10.1002/pmic.201500010.
[59] K. Yoneda, M. Yoshida, I. Suzuki, M.M. Watanabe, Identification of a major lipid droplet protein in a marine diatom *Phaeodactylum tricornutum*, Plant Cell Physiol. 57 (2016) 397–406, https://doi.org/10.1093/pcp/pcv204.
[60] P.K. Chiang, R.K. Gordon, J. Tal, G.C. Zeng, B.P. Doctor, K. Pardhasaradhi, P.P. McCann, S-adenosylmethionine and methylation, FASEB J. 10 (1996) 471–480.
[61] E. Martinoia, M. Maeshima, H.E. Neuhaus, Vacuolar transporters and their essential role in plant metabolism, J. Exp. Bot. 58 (2007) 83–102, https://doi.org/10.1093/jxb/erl183.
[62] A. Marchetti, D.M. Schruth, C.A. Durkin, M.S. Parker, R.B. Kodner, C.T. Berthiaume, R. Morales, A.E. Allen, E.V. Armbrust, Comparative metatranscriptomics identifies molecular bases for the physiological responses of phytoplankton to varying iron availability, Proc. Natl. Acad. Sci. 109 (2012) E317–E325, https://doi.org/10.1073/pnas.1118408109.
[63] J.B. McQuaid, A.B. Kustka, M. Oborník, A. Horák, J.P. McCrow, B.J. Karas, H. Zheng, T. Kindeberg, A.J. Andersson, K.A. Barbeau, A.E. Allen, Carbonate-sensitive phytotransferrin controls high-affinity iron uptake in diatoms, Nature 555 (2018) 534–537, https://doi.org/10.1038/nature25982.
[64] D. Vaulot, R.J. Olson, S.M. Merkel, S.W. Chisholm, Cell cycle response to nutrient starvation in two marine phytoplankton species, Mar. Biol. 95 (1987) 625–630.
[65] P. Claquin, V. Martin-Jézéquel, J.C. Kromkamp, M.J.W. Veldhuis, G.W. Kraay, Uncoupling of silicon compared with carbon and nitrogen metabolisms and the role of the cell cycle in continuous cultures of *Thalassiosira pseudonana* (Bacillariophyceae) under light, nitrogen, and phosphorus control, J. Phycol. 38 (2002) 922–930, https://doi.org/10.1046/j.1529-8817.2002.t01-1-01220.x.
[66] J. Kim, C.M. Brown, M.K. Kim, E.H. Burrows, S. Bach, D.S. Lun, P.G. Falkowski, Effect of cell cycle arrest on intermediate metabolism in the marine diatom *Phaeodactylum tricornutum*, Proc. Natl. Acad. Sci. 201711642 (2017), https://doi.org/10.1073/pnas.1711642114.
[67] L.T. Guerra, O. Levitan, M.J. Frada, J.S. Sun, P.G. Falkowski, G.C. Dismukes, Regulatory branch points affecting protein and lipid biosynthesis in the diatom *Phaeodactylum tricornutum*, Biomass Bioenergy 59 (2013) 306–315, https://doi.org/10.1016/j.biombioe.2013.10.007.
[68] H. Wagner, T. Jakob, J. Lavaud, C. Wilhelm, Photosystem II cycle activity and alternative electron transport in the diatom *Phaeodactylum tricornutum* under dynamic light conditions and nitrogen limitation, Photosynth. Res. 128 (2015) 1–11, https://doi.org/10.1007/s11120-015-0209-7.
[69] L. Chunying, Production of dimethylsulfi de and acrylic acid from dimethylsulfoniopropionate during growth of three marine microalgae*, Chin. J. Oceanol. Limnol. 32 (2014) 1270–1279, https://doi.org/10.1007/s00343-015-4029-6.
[70] J. Popko, C. Herrfurth, K. Feussner, T. Ischebeck, T. Iven, R. Haslam, M. Hamilton, O. Sayanova, J. Napier, I. Khozin-Goldberg, I. Feussner, Metabolome analysis reveals betaine lipids as major source for triglyceride formation, and the accumulation of sedoheptulose during nitrogen-starvation of *Phaeodactylum tricornutum*, PLoS One 11 (2016) 1–23, https://doi.org/10.1371/journal.pone.0164673.
[71] D.M. Slezak, S. Puskaric, G.J. Herndl, Potential role of acrylic acid in bacterioplankton communities in the sea, Mar. Ecol. Prog. Ser. 105 (1994) 191–197.
[72] E. Bucciarelli, W.G. Sunda, Influence of CO2, nitrate, phosphate, and silicate limitation on intracellular dimethylsulfoniopropionate in batch cultures of the coastal diatom *Thalassiosira pseudonana*, Limnol. Oceanogr. 48 (2003) 2256–2265, https://doi.org/10.4319/lo.2003.48.6.2256.
[73] L. Alipanah, J. Rohloff, P. Winge, A.M. Bones, T. Brembu, Whole-cell response to nitrogen deprivation in the diatom *Phaeodactylum tricornutum*, J. Exp. Bot. 66 (2015) 6281–6296, https://doi.org/10.1093/jxb/erv340.
[74] O. Levitan, J. Dinamarca, E. Zelzion, D.S. Lun, L.T. Guerra, M.K. Kim, J. Kim, B.A.S. Van Mooy, D. Bhattacharya, P.G. Falkowski, Remodeling of intermediate metabolism in the diatom *Phaeodactylum tricornutum* under nitrogen stress, Proc. Natl. Acad. Sci. U. S. A. 112 (2015) 412–417, https://doi.org/10.1073/pnas.1419818112.
[75] C. Shang, S. Zhu, Z. Wang, L. Qin, M.A. Alam, J. Xie, Z. Yuan, Proteome response of *Dunaliella parva* induced by nitrogen limitation, Algal Res. 23 (2017) 196–202, https://doi.org/10.1016/j.algal.2017.01.016.
[76] S.M. Dittami, G. Michel, J. Collén, C. Boyen, T. Tonon, Chlorophyll-binding proteins revisited - a multigenic family of light-harvesting and stress proteins from a brown algal perspective, BMC Evol. Biol. 10 (2010) 365, https://doi.org/10.1186/1471-2148-10-365.
[77] M. Nymark, K.C. Valle, K. Hancke, P. Winge, K. Andresen, G. Johnsen, A.M. Bones, T. Brembu, Molecular and photosynthetic responses to prolonged darkness and subsequent acclimation to re-illumination in the diatom *Phaeodactylum tricornutum*, PLoS One 8 (2013), https://doi.org/10.1371/journal.pone.0058722.
[78] S.H. Zhu, B.R. Green, Photoprotection in the diatom *Thalassiosira pseudonana*: role of LI818-like proteins in response to high light stress, Biochim. Biophys. Acta Bioenerg. 1797 (2010) 1449–1457, https://doi.org/10.1016/j.bbabio.2010.04.003.
[79] M. Nymark, K.C. Valle, T. Brembu, K. Hancke, P. Winge, K. Andresen, G. Johnsen, A.M. Bones, An integrated analysis of molecular acclimation to high light in the marine diatom *Phaeodactylum tricornutum*, PLoS One 4 (2009), https://doi.org/10.1371/journal.pone.0007743.
[80] N. Domingues, A.R. Matos, J. Marques da Silva, P. Cartaxana, Response of the diatom *Phaeodactylum tricornutum* to photooxidative stress resulting from high light exposure, PLoS One 7 (2012), https://doi.org/10.1371/journal.pone.0038162.
[81] E. Erickson, S. Wakao, K.K. Niyogi, Light stress and photoprotection in *Chlamydomonas reinhardtii*, Plant J. 82 (2015) 449–465, https://doi.org/10.1111/tpj.12825.
[82] I.M. Remmers, D.E. Martens, R.H. Wijffels, P.P. Lamers, Dynamics of triacylglycerol and EPA production in *Phaeodactylum tricornutum* under nitrogen starvation at different light intensities, PLoS One 12 (2017) e0175630, , https://doi.org/10.1371/journal.pone.0175630.
[83] A.E. Allen, C.L. Dupont, M. Oborník, A. Horák, A. Nunes-Nesi, J.P. McCrow, H. Zheng, D.A. Johnson, H. Hu, A.R. Fernie, C. Bowler, Evolution and metabolic significance of the urea cycle in photosynthetic diatoms, Nature 473 (2011) 203–207, https://doi.org/10.1038/nature10074.
[84] T. Obata, A.R. Fernie, A. Nunes-Nesi, The central carbon and energy metabolism of marine diatoms, Metabolites 3 (2013) 325–346, https://doi.org/10.3390/metabo3020325.
[85] M. Matthijs, M. Fabris, T. Obata, I. Foubert, J.M. Franco-Zorrilla, R. Solano, A.R. Fernie, W. Vyverman, A. Goossens, The transcription factor bZIP14 regulates the TCA cycle in the diatom *Phaeodactylum tricornutum*, EMBO J. 36 (2017) 1559–1576, https://doi.org/10.15252/embj.201696392.
[86] O. Levitan, J. Dinamarca, E. Zelzion, D.S. Lun, L.T. Guerra, M.K. Kim, J. Kim, B.A.S. Van Mooy, D. Bhattacharya, P.G. Falkowski, Remodeling of intermediate metabolism in the diatom *Phaeodactylum tricornutum* under nitrogen stress, Proc. Natl. Acad. Sci. 112 (2015) 412–417, https://doi.org/10.1073/pnas.1419818112.
[87] M.A. Caballero, D. Jallet, L. Shi, C. Rithner, Y. Zhang, G. Peers, Quantification of chrysolaminarin from the model diatom *Phaeodactylum tricornutum*, Algal Res. 20 (2016) 180–188, https://doi.org/10.1016/j.algal.2016.10.008.
[88] O. Sayanova, V. Mimouni, L. Ulmann, A. Morant-Manceau, V. Pasquet, B. Schoefs, J.A. Napier, Modulation of lipid biosynthesis by stress in diatoms, Philos. Trans. R. Soc. B 372 (2017), https://doi.org/10.1098/rstb.2016.0407.
[89] X. Wang, Z. Shen, X. Miao, Nitrogen and hydrophosphate affects glycolipids composition in microalgae, Sci. Rep. 6 (2016) 1–9, https://doi.org/10.1038/srep30145.
[90] P.G. Kroth, A. Chiovitti, A. Gruber, V. Martin-Jezequel, T. Mock, M.S. Parker, M.S. Stanley, A. Kaplan, L. Caron, T. Weber, U. Maheswari, E.V. Armbrust, C. Bowler, A model for carbohydrate metabolism in the diatom *Phaeodactylum tricornutum* deduced from comparative whole genome analysis, PLoS One 3 (2008)

e1426, , https://doi.org/10.1371/journal.pone.0001426.
[91] Y. Tsuji, A. Mahardika, Y. Matsuda, Evolutionarily distinct strategies for the acquisition of inorganic carbon from seawater in marine diatoms, J. Exp. Bot. 68 (2017) 3949–3958, https://doi.org/10.1093/jxb/erx102.
[92] M. Fabris, M. Matthijs, S. Rombauts, W. Vyverman, A. Goossens, G.J.E. Baart, The metabolic blueprint of *Phaeodactylum tricornutum* reveals a eukaryotic Entner-Doudoroff glycolytic pathway, Plant J. 70 (2012) 1004–1014, https://doi.org/10.1111/j.1365-313X.2012.04941.x.
[93] M.F. Liaud, C. Lichtle, K. Apt, W. Martin, R. Cerff, Compartment-specific isoforms of TPI and GAPDH are imported into diatom mitochondria as a fusion protein: evidence in favor of a mitochondrial origin of the eukaryotic glycolytic pathway, Mol. Biol. Evol. 17 (2000) 213–223, https://doi.org/10.1093/oxfordjournals.molbev.a026301.
[94] M.S. Chauton, P. Winge, T. Brembu, O. Vadstein, A.M. Bones, Gene regulation of carbon fixation, storage, and utilization in the diatom *Phaeodactylum tricornutum* acclimated to light/dark cycles, Plant Physiol. 161 (2013) 1034–1048, https://doi.org/10.1104/pp.112.206177.
[95] S.R. Smith, R.M. Abbriano, M. Hildebrand, Comparative analysis of diatom genomes reveals substantial differences in the organization of carbon partitioning pathways, Algal Res. 1 (2012) 2–16, https://doi.org/10.1016/j.algal.2012.04.003.
[96] P.G. Kroth, Genetic transformation: a tool to study protein targeting in diatoms, Methods Mol. Biol. 390 (2007) 257–267.
[97] O. Levitan, J. Dinamarca, E. Zelzion, M.Y. Gorbunov, P.G. Falkowski, An RNA interference knock-down of nitrate reductase enhances lipid biosynthesis in the diatom *Phaeodactylum tricornutum*, Plant J. 84 (2015) 963–973, https://doi.org/10.1111/tpj.13052.
[98] Y. Gong, J. Zhang, X. Guo, X. Wan, Z. Liang, C.J. Hu, M. Jiang, Identification and characterization of PtDGAT2B, an acyltransferase of the DGAT2 acyl-coenzyme A: diacylglycerol acyltransferase family in the diatom *Phaeodactylum tricornutum*, FEBS Lett. 587 (2013) 481–487, https://doi.org/10.1016/j.febslet.2013.01.015.
[99] F. Guihéneuf, S. Leu, A. Zarka, I. Khozin-Goldberg, I. Khalilov, S. Boussiba, Cloning and molecular characterization of a novel acyl-CoA:diacylglycerol acyltransferase 1-like gene (PtDGAT1) from the diatom *Phaeodactylum tricornutum*, FEBS J. 278 (2011) 3651–3666, https://doi.org/10.1111/j.1742-4658.2011.08284.x.
[100] J. Dinamarca, O. Levitan, G.K. Kumaraswamy, D.S. Lun, P.G. Falkowski, Overexpression of a diacylglycerol acyltransferase gene in *Phaeodactylum tricornutum* directs carbon towards lipid biosynthesis, J. Phycol. 53 (2017) 405–414, https://doi.org/10.1111/jpy.12513.
[101] F. Ge, W. Huang, Z. Chen, C. Zhang, Q. Xiong, C. Bowler, J. Yang, J. Xu, H. Hu, Methylcrotonyl-CoA Carboxylase regulates triacylglycerol accumulation in the model diatom *Phaeodactylum tricornutum*, Plant Cell 26 (2014) 1681–1697, https://doi.org/10.1105/tpc.114.124982.
[102] J.-J. Park, H. Wang, M. Gargouri, R.R. Deshpande, J.N. Skepper, F.O. Holguin, M.T. Juergens, Y. Shachar-Hill, L.M. Hicks, D.R. Gang, The response of *Chlamydomonas reinhardtii* to nitrogen deprivation: a systems biology analysis, Plant J. 81 (2015) 611–624, https://doi.org/10.1111/tpj.12747.
[103] E.C. Goncalves, J.V. Johnson, B. Rathinasabapathi, Conversion of membrane lipid acyl groups to triacylglycerol and formation of lipid bodies upon nitrogen starvation in biofuel green algae *Chlorella* UTEX29, Planta 238 (2013) 895–906, https://doi.org/10.1007/s00425-013-1946-5.